Journal of Medicinal Chemistry

Subscriber access provided by UNIV OF NEBRASKA - LINCOLN

Article

Discovery and Evaluation of Clinical Candidate AZD3759, a Potent, Oral Active, Central Nervous System-Penetrant, Epidermal Growth Factor Receptor Tyrosine Kinase Inhibitor (EGFR TKI)

Qingbei Zeng, Jiabing Wang, Ziqiang Cheng, Kan Chen, Peter Johnström, Katarina Varnas, David Yunzhi Li, Zhen Fan Yang, and Xiaolin Zhang

J. Med. Chem., **Just Accepted Manuscript** • DOI: 10.1021/acs.jmedchem.5b01073 • Publication Date (Web): 27 Aug 2015

Downloaded from http://pubs.acs.org on August 28, 2015

Just Accepted

"Just Accepted" manuscripts have been peer-reviewed and accepted for publication. They are posted online prior to technical editing, formatting for publication and author proofing. The American Chemical Society provides "Just Accepted" as a free service to the research community to expedite the dissemination of scientific material as soon as possible after acceptance. "Just Accepted" manuscripts appear in full in PDF format accompanied by an HTML abstract. "Just Accepted" manuscripts have been fully peer reviewed, but should not be considered the official version of record. They are accessible to all readers and citable by the Digital Object Identifier (DOI®). "Just Accepted" is an optional service offered to authors. Therefore, the "Just Accepted" Web site may not include all articles that will be published in the journal. After a manuscript is technically edited and formatted, it will be removed from the "Just Accepted" Web site and published as an ASAP article. Note that technical editing may introduce minor changes to the manuscript text and/or graphics which could affect content, and all legal disclaimers and ethical guidelines that apply to the journal pertain. ACS cannot be held responsible for errors or consequences arising from the use of information contained in these "Just Accepted" manuscripts.

ACS Publications

Journal of Medicinal Chemistry is published by the American Chemical Society. 1155 Sixteenth Street N.W., Washington, DC 20036

Published by American Chemical Society. Copyright © American Chemical Society. However, no copyright claim is made to original U.S. Government works, or works produced by employees of any Commonwealth realm Crown government in the course of their duties.

Discovery and Evaluation of Clinical Candidate AZD3759, a Potent, Oral Active, Central Nervous System-Penetrant, Epidermal Growth Factor Receptor Tyrosine Kinase Inhibitor (EGFR TKI)

Qingbei Zeng[1], Jiabing Wang[1], Ziqiang Cheng[1], Kan Chen[1], Peter Johnström[2,3], Katarina Varnäs[3], David Yunzhi Li[1], Zhen Fan Yang[1], Xiaolin Zhang[1,]*

[1]Innovation Center China, Asia & Emerging Markets iMed, AstraZeneca Innovative Medicines and Early Development, 199 Liangjing Road, Zhangjiang Hi-Tech Park, Shanghai 201203, China

[2]AstraZeneca Translational Centre, Personal Healthcare and Biomarkers iMed, AstraZeneca R&D, Karolinska Institutet, Department of Clinical Neuroscience, R5:U1 Karolinska University Hospital, SE-171 76 Stockholm, Sweden

[3]Karolinska Institutet, Department of Clinical Neuroscience, Centre for Psychiatry Research, R5:02 Karolinska University Hospital, SE-171 76 Stockholm, Sweden

ABSTRACT: Recent reports suggest that an increasing number of patients with lung cancer, especially those with activating mutations of the epidermal growth factor receptor (EGFR), also

present with brain metastases (BM) and leptomeningeal metastases (LM). These patients have poor prognosis as there are no approved drugs for these indications. Available agents have poor efficacy for these patients even at well above their standard dose. Herein we report the discovery of (4-[(3-chloro-2-fluorophenyl)amino]-7-methoxyquinazolin-6-yl (*2R*)-2,4-dimethylpiperazine-1-carboxylate **1m** (AZD3759), an investigational drug currently in Phase 1 clinical trial, which has excellent central nervous system (CNS) penetration and which induced profound regression of brain metastases in a mouse model.

▪ INTRODUCTION

Non-small cell lung cancer (NSCLC) accounts for more than 85% of all lung cancer cases and is one of the leading causes of cancer death worldwide.[1] It is estimated that in 2014 there were 224,210 new lung cancer cases and 159,260 NSCLC related deaths in the United States alone.[2] Genetic aberrations in the tyrosine kinase domain of epidermal growth factor receptor have been identified as one of the key drivers of NSCLC progression.[3] EGFR kinase inhibitors, such as gefitinib, erlotinib, and afatinib (**Scheme 1**), deliver significant patient benefit and have been approved for the treatment of advanced NSCLC with EGFR activating mutations.[4-7]

An increased incidence of CNS metastases has been reported as patients live longer with treatment and with the improvement of imaging technology and routine screening.[8,9] Studies have suggested that around 40-50% of patients with lung cancer would develop CNS metastases, including brain metastases and leptomeningeal metastases, in their life span.[10,11] Currently approved drugs can neither effectively treat lung cancer CNS metastases nor prevent development of the metastases at standard dosing due to their limited blood-brain-barrier (BBB) penetration.[12,13] For patients with symptomatic brain metastases, selective use of radiation therapy and surgery are still the mainstay of treatment but provide limited benefit.[14,15] Given the

effectiveness of EGFR TKIs in treating tumors in the lung, there is a major unmet medical need for an agent which can effectively penetrate the CNS and treat tumors in this tissue.

Scheme 1. Approved EGFR Kinase Inhibitors

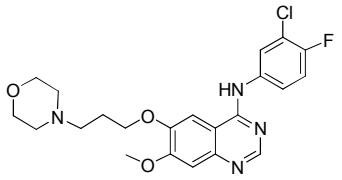

Gefitinib

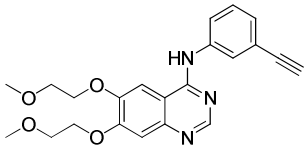

Erlotinib

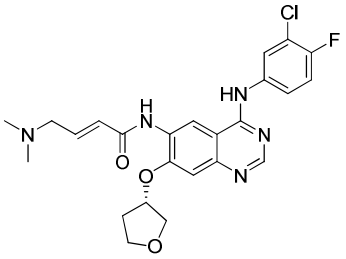

Afatinib

▪ RESULTS AND DISCUSSION

Discovery of compound 1m. In order to achieve efficacy in the CNS and periphery, it is necessary to design biologically active agents with sufficient free drug exposures in both environments. Initially, we started with the clinically proven EGFR TKI gefitinib, developed by AstraZeneca, as the lead for the project with the objective of developing a CNS penetrable candidate with potency and selectivity equal to or better than gefitinib.

It has been a challenging task to deliver a pharmaceutical agent that can enter the CNS.[16] Efflux transport is a major determinant of drug disposition to the CNS. ATP-binding cassette (ABC) export proteins such as P-glycoprotein (Pgp) and breast cancer resistance protein (BCRP) are localized in the luminal membrane of brain microvessel endothelial cells.[17,18] Pgp and BCRP have been shown to play an important role in limiting distribution of various drugs into the CNS. We examined several key parameters related to BBB penetration for approved EGFR inhibitors (see Supporting Information for experimental protocols). **Table 1** summarizes physicochemical properties, unbound brain to unbound blood ratios ($K_{puu,brain}$), cerebrospinal fluid (CSF) to

unbound blood ratios ($K_{puu,CSF}$), and efflux ratios of these compounds in MDCKII-MDR1 and MDCKII-BCRP permeability experiments. All these agents are either Pgp (MDR1) or BCRP substrates such that their $K_{puu,brain}$ or $K_{puu,CSF}$ values are low. Unfavorable rotatable bonds in gefitinib (10 rotatable bonds) and erlotinib (11 rotatable bonds) and undesired hydrogen bond donors in afatinib (2 hydrogen bond donors) are likely responsible for the low CNS penetration of these agents. Recently published papers highlighted that the correct balance of permeability, potential for active efflux, and physicochemical properties, is needed to achieve good drug partitioning and distribution into CNS with CNS active drugs having lower molecular weight, fewer rotatable bonds, smaller polar surface area (PSA), and fewer hydrogen bond donors than non-CNS-penetrant drugs.[19-23]

Table 1. Physicochemical Properties, Permeability and CNS Penetration Properties of Approved EGFR Kinase Inhibitors

		Gefitinib	Erlotinib	Afatinib
Molecular weight		446.7	393.4	485.9
tPSA (Å^2)		62.6	70.3	86.1
Rotatable bonds[a]		10	11	9
Hydrogen bond donor number		1	1	2
MDCKII-MDR1[b]	$P_{app,\ A\ to\ B}$ (10^{-6} cm/s)	8.3	19	2.5
	Efflux ratio[c]	3.0	1.7	11
MDCKII-BCRP[d]	$P_{app,\ A\ to\ B}$ (10^{-6} cm/s)	4.2	14	1.3
	Efflux ratio[c]	18	5.4	59
$f_{u,blood}$ (%)[e]		3.3	4.5	4.1
$f_{u,brain}$ (%)[f]		0.39	2.9	0.54
$K_{puu,brain}$[g]		0.021	0.11	0.0066
$K_{puu,CSF}$[h]		0.088	0.29	0.27

[a]Rotatable bond number is calculated by the equation of $N_{rot} = N_{rot,ac} + \Sigma(size - 4 - N_{ring,ac} - N_{fused})$, where N_{rot} is rotatable bond number in the molecule, $N_{rot,ac}$ is the number of rotatable acyclic bonds, *Size* is the size of the non-aromatic ring, $N_{rig,cyc}$ is the number of rigid bonds within the ring and N_{fused} is the number of bonds which belong to more than one ring system. [b]Permeability was estimated by using MDR1-transfected MDCKII cells seeded onto polyethylene membranes in 96-well BD insert systems with test compounds at 1 μM. [c]Efflux ratio = $P_{app,B\ to\ A}$/ $P_{app,A\ to\ B}$. [d]Permeability was estimated by using BCRP-transfected MDCKII cells seeded onto polyethylene membranes in 96-well BD insert systems

with test compounds at 1 μM.). [e]Fraction of unbound drug in blood was obtained with the test compound at 5 μM by equilibrium dialysis. [f]Fraction of unbound drug in brain homogenate was obtained with the test compound at 5 μM by equilibrium dialysis. [g]Ratio of unbound $AUC_{0\text{-}24h}$ in rat brain to that in blood at the clinically relevant dose of EGFR TKIs. [h]Ratio of $AUC_{0\text{-}24h}$ in rat CSF to unbound $AUC_{0\text{-}24h}$ in blood at the clinical relevant dose of EGFR TKIs, see Supporting Information for more details.

Achieving these desirable physicochemical properties while retaining good EGFR TKI potency was the challenge. X-ray structure analysis of the gefitinib-EGFR complex indicated that the quinazoline positions a hydrogen bond acceptor to Met793 in the hinge region of EGFR and the anilino substituent extends into the hydrophobic pocket at the back of the ATP-binding cleft.[24] These structural elements, therefore, are essential to EGFR inhibitor activity and hence we decided to retain this template but to re-engineer the quinazoline-based molecules to deliver the physicochemical properties needed for CNS penetration, initially by re-directing the fluoro moiety present in the phenyl group from the *para* to *ortho* position (**Scheme 2**). The previous SAR study at AstraZeneca indicated that re-positioning fluorine atom present in gefitinib from the *para* position to the *ortho* position maintained EGFR kinase inhibitory potency.[25] It was believed that *ortho*-fluorine atom could partially mask the hydrogen bond donating effect of the N-H by forming an intramolecular interaction.[26-28] Additionally, the linear and rotatable side chain present in gefitinib was shortened to derive molecules with the general structure **1** (**Scheme 2**).

Scheme 2. Design Strategy Starting from Gefitinib as an Initial Lead

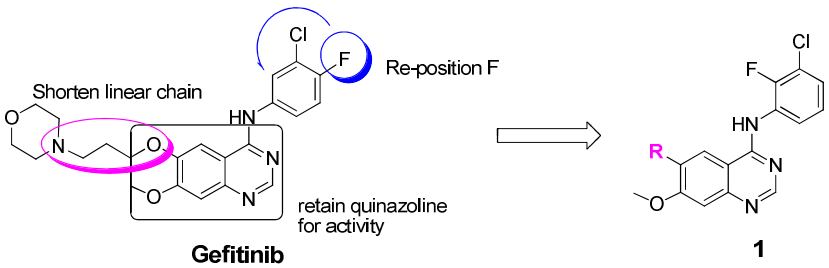

The brain and CSF penetration of the agents was estimated by $K_{puu,brain}$ and $K_{puu,CSF}$, respectively.[29,30] $K_{puu,brain}$ is the ratio of unbound AUC in brain to unbound AUC in blood and

$K_{puu,CSF}$ is the ratio of AUC in CSF to unbound AUC in blood (see Supporting Information for more details). Compared to gefitinib, compound **1a** has lower molecular weight and polar surface area (**Table 2**) and is also a more rigid molecule (seven rotatable bonds) than gefitinib (ten rotatable bonds). As a result, CNS drug-like properties, such as efflux ratio (0.33) and permeability ($P_{app,A\ to\ B}$ = 32 x 10^{-6} cm/s) were achieved. Encouragingly, this compound exhibited inhibitory potency (IC_{50}) at 3.8 nM and 6.6 nM in PC-9 and H3255 cell line EGFR phosphorylation assays, which were comparable to that of gefitinib (at 6.2 nM and 6.5 nM, respectively). Furthermore, compound **1a** demonstrated acceptable human CYP450 inhibition profile (IC_{50} > 10 μM for CYP2C9, CYP2D6 and CYP3A4) and low hERG inhibition liability (hERG IC_{50} = 17 μM, patch clamp assay). More importantly, the preferred CNS drug-like properties of the compound translated into much improved brain and CSF penetration ($K_{puu,brain}$ and $K_{puu,CSF}$ were 0.47 and 0.76, respectively) and reasonable exposures in both brain and blood ($AUC_{0\text{-}7h}$ values in brain and blood at 2 mg/kg were 1013 nM·h and 834 nM·h, respectively) were achieved. These excellent *in vitro* potency and promising CNS penetration results were achieved while maintaining a reasonable pharmacokinetic (PK) properties in rat (oral bioavailability 44%, elimination half-life 1.1 hours, clearance 59 mL/min/kg and volume of distribution at steady state 2.8 L/kg). With these encouraging results, further reduction in the molecular weight and the number of rotatable bonds of **1a** led to **1b**. As expected, this compound benefits from increased $K_{puu,brain}$ and $K_{puu,CSF}$ (0.96 and 0.93, respectively). In order to examine the importance of the position of the fluorine atom, inhibitor **2** with a *para* substituent was prepared. Comparison of **1b** with **2** suggested that indeed the intramolecular interaction between the fluoro and N-H in **1b** is important for CNS penetration. However, agents **1b** and **2** also showed substantially lower level of blood and brain AUCs compared with **1a**. As

subsequent attempts to modify either **1b** or **2** did not lead to further improvement in PK properties, **1b** and **2** analogs were no longer pursued and optimization of **1a** became the priority. In order to improve the PK properties of **1a**, the next effort was to modify the potentially labile methylene group (**Table 2**). An initial attempt was to change the methylene unit into a carbonyl moiety (**1c**) which could reduce potential oxidative liability and further decrease the bond rotation. Unfortunately, this compound (**1c**) was not a CNS penetrant and was much less potent in a cell based phosphorylation assay (L858R pEGFR IC_{50} = 166 nM). However, an extension of the amide present in **1c** by one atom to give the carbamate (**1d**) significantly improved potency (L858R pEGFR IC_{50} = 4.1 nM), although the exposures of **1d** in brain and plasma were very low (**Table 2**). The poor equilibrium solubility (12 nM in pH 7.4 buffer) of the compound was identified as a potential limiting factor for oral exposure. Thus, further modification were undertaken to replace the oxygen present in the morpholine ring at the terminal position with a basic nitrogen (**1e**). Indeed, the solubility of **1e** (free base) was increased substantially (202 mM in neutral buffer). With this increase in basicity (pKa = 8.4) and solubility, the exposure of **1e** in brain and blood improved dramatically.

Table 2. Results from Optimizing Physicochemical Properties

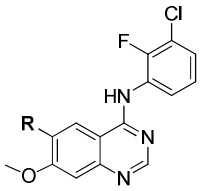

1a-e

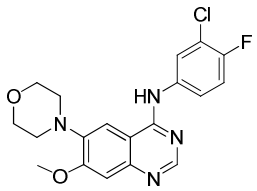

2

Compounds	Gefitinib	1a	1b	1c	1d	1e	2
R =	--					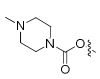	--
Molecular weight	446.7	402.9	388.8	416.8	432.8	445.9	388.8

tPSA (Å^2)	62.6	53.5	53.2	71.8	80.9	73.3	53.2
Rotatable bonds[a]	10	7	6	6	6	6	6
L858R pEGFR IC_{50} (nM)[b]	6.5	6.6	1.5	166.0	4.1	5.0	1.5
MDCKII-MDR1 $P_{app,\ A\ to\ B}$ (10^{-6} cm/s)[c]	8.3	32	32	28	42	28	29
Efflux ratio[d]	3.0	0.33	0.29	2.9	0.58	0.37	0.18
Brain $AUC_{0\text{-}7h}$ (nM·h)[e]	5647[f]	1013	85	101	104	825	85
CSF $AUC_{0\text{-}7h}$ (nM·h)[e]	93[f]	50	2	46	5	31	1
Blood $AUC_{0\text{-}7h}$ (nM·h)[e]	31913[f]	834	33	1627	42	722	77
$f_{u,blood}$ (%)[g]	3.3	7.8	5.8	17	3.8	8.4	2.2
$f_{u,brain}$ (%)[h]	0.39	3.0	2.2	8.8	2.6	2.5	0.83
$K_{puu,brain}$[i]	0.021[j]	0.47	0.96	0.03	1.7	0.34	0.42
$K_{puu,CSF}$[k]	0.088[l]	0.76	0.93	0.16	3.4	0.52	0.79

[a]Rotatable bond number is calculated by the equation of $N_{rot} = N_{rot,ac} + \Sigma(size - 4 - N_{ring,ac} - N_{fused})$, where N_{rot} is rotatable bond number in the molecule, $N_{rot,ac}$ is the number of rotatable acyclic bonds, *Size* is the size of the non-aromatic ring, $N_{rig,cyc}$ is the number of rigid bonds within the ring and N_{fused} is the number of bonds which belong to more than one ring system. [b]Cellular phosphorylation assay on H3255 (L858R) cell lines (n = 2). [c]MDR1-transfected MDCKII cells with test compound at 1 μM were used to estimate apical to basolateral permeability. [d]Efflux ratio = $P_{app,\ B\ to\ A}$/ $P_{app,\ A\ to\ B}$. [e]Male Han Wistar rats (PO, 2 mg/kg; 1% MC). [f]Clinically equivalent dose of 20 mg/kg was orally administrated for CNS penetration assessment of gefitinib and exposure was measured between 0.5 and 24 hr. [g]Fraction of unbound drug in blood was obtained with the test compound at 5 μM by equilibrium dialysis. [h]Fraction of unbound drug in brain homogenate was obtained with the test compound at 5μM by equilibrium dialysis. [i]Ratio of unbound brain $AUC_{0\text{-}7h}$ to unbound blood $AUC_{0\text{-}7h}$. [j]Ratio of unbound brain $AUC_{0\text{-}24h}$ to unbound blood $AUC_{0\text{-}24h}$. [k]Ratio of CSF $AUC_{0\text{-}7h}$ to unbound blood $AUC_{0\text{-}7h}$. [l]Ratio of CSF $AUC_{0\text{-}24h}$ to unbound blood $AUC_{0\text{-}24h}$.

Given its promising *in vitro* potency and good brain penetration, a rat PK study was conducted for compound **1e** and the results are summarized in **Table 3**. Compared to **1a**, inhibitor **1e** significantly improved clearance (22 mL/min/kg) in rat. It was quickly absorbed and the oral bioavailability was 45% while the elimination half-life was increased to 2.6 h. This improved half-life, however, did not meet our design criteria (>4 h in rat).

Table 3. Rat PK Data for Compound **1e**[a]:

Dose (route)	Formulation	$AUC_{0\text{-}24h}$ (nM·h)[b]	F (%)[c]	$T_{1/2}$ (h)[d]	T_{max} (h)[e]	C_{max} (nM)[f]	CL (mL/min/kg)[g]	V_{ss} (L/kg)[h]
5 mg/kg (PO)	1% methylcellulose	3905	45	--	0.25	2020	--	--
1 mg/kg (iv)	DMSO:10% Captisol in saline = 1:99	1713	--	2.6	--	--	22	1.8

[a]Male Han Wistar rats (non-fasted) were used in this study. [b]Area under concentration-time curve from 0-24 hours. [c]Bioavailability (%). [d]Mean elimination half-life. [e]Time to reach maximum concentration. [f]Peak concentration. [g]Clearance, obtained from intravenous infusion. [h]Volume of distribution at steady state. All pharmacokinetic parameters were calculated with Phoenix v6.3 (Certara, St Louis, MO, USA).

Table 4. Properties of Compounds **1f-n**.

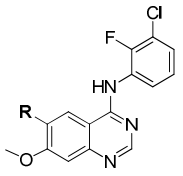

1f-n

Compounds	**1f**	**1g**	**1h**	**1i**	**1j**	**1k**	**1l**	**1m**	**1n**
R =	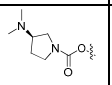	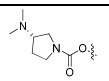	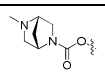	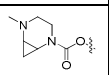 isomer 1	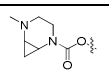 isomer 2	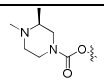	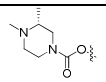	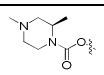	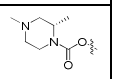
Rotatable bonds[a]	6	6	4	5	5	6	6	6	6
L858R pEGFR IC_{50} (nM)[b]	1.1	2.7	2.3	4.4	12.8	16.9	21.5	7.2	6.9
MDCKII-MDR1 $P_{app, A\ to\ B}$ (10^{-6} cm/s)[c]	47	17	14	67	76	59	54	36	51
Efflux ratio[d]	0.76	0.34	0.39	0.60	0.69	1.5	0.94	0.41	0.92
Brain $AUC_{0\text{-}7h}$ (nM·h)[e]	2037	798	332	585[f]	727[f]	278	417	3692	1935
CSF $AUC_{0\text{-}7h}$ (nM·h)[e]	75	68	BQL[g]	19[f]	28[f]	19	7	76	48
Blood $AUC_{0\text{-}7h}$ (nM·h)[e]	3001	2483	454	786[f]	740[f]	157	404	1231	805
$f_{u,blood}$ (%)[h]	5.8	4.9	13.4	2.8	2.4	3.5	6.4	4.7[i]	2.3
$f_{u,brain}$ (%)[j]	2.3	2.4	1.6	1.9	1.8	1.6	1.8	2.0[i]	1.5
$K_{puu,brain}$[k]	0.27	0.15	0.086	0.51	0.74	0.84	0.28	1.3	1.6
$K_{puu,CSF}$[l]	0.43	0.56	BQL[g]	0.90	1.6	3.5	0.28	1.3	2.6

[a]Rotatable bond number is calculated by the equation of $N_{rot} = N_{rot,ac} + \Sigma(size - 4 - N_{ring,ac} - N_{fused})$, where N_{rot} is rotatable bond number in the molecule, $N_{rot,ac}$ is the number of rotatable acyclic bonds, *Size* is the size of the non-aromatic ring, $N_{rig,cyc}$ is the number of rigid bonds within the ring and N_{fused} is the number of bonds which belong to more than one ring system. [b]Cellular phosphorylation assay on H3255 (L858R) cell lines (n = 2). [c]MDR1-transfected MDCKII cells with the test compound at 1 μM were used to estimate apical to basolateral permeability. [d]Efflux ratio = $P_{app, B\ to\ A}$/ $P_{app, A\ to\ B}$. [e]Male Han Wistar rats (PO, 2 mg/kg; 1% MC. [f]$AUC_{0\text{-}6.5h}$. [g]Compound **1h** concentrations in CSF at predefined time points were below the quantification limit (1 ng/mL).). [h]Fraction of unbound drug in blood was obtained with test compound at 5μM by equilibrium dialysis. [i]Average value from 4 independent tests. [j]Fraction of unbound drug in brain homogenate was obtained with the test compound at 5 μM by equilibrium dialysis. [k]Ratio of unbound brain $AUC_{0\text{-}7h}$ to unbound blood $AUC_{0\text{-}7h}$. [l]Ratio of CSF $AUC_{0\text{-}7h}$ to unbound blood $AUC_{0\text{-}7h}$.

The subsequent **1e** metabolite identification in rat hepatocytes suggested that piperazine oxidation was the main metabolic pathway (see Supporting Information for more details). Thus, introduction of substituent(s) to the piperazine ring or change of the piperazine to another moiety was examined (**Table 4**). Initially, we designed compounds **1f** and **1g** by replacing the piperazine with a dimethylaminopyrrolidine moiety. These pyrrolidine derivatives (**1f** and **1g**) displayed

excellent potency (IC_{50} = 1.1 nM and 2.7 nM, respectively) in cellular EGFR phosphorylation assays but whilst blood AUC levels of these compounds were also increased and their levels of brain penetration were not acceptable ($K_{puu,brain}$ < 0.3). The limited brain penetration is potentially due to the increased flexibility from the rotatable bond between the terminal dimethylamino and pyrrolidine ring. Hence subsequently, the piperazine was substituted by a much more rigid bridged bicyclic system. The constrained analog **1h** (four rotatable bonds) showed further reduced CNS penetration ($K_{puu,brain}$ and $K_{puu,CSF}$ < 0.1) which led us to speculate that a balanced molecular flexibility (rotatable bond number) is needed for favorable CNS penetration. Thus, compounds **1i-n** were designed and prepared. In these compounds, the rotatable bond numbers were retained at a range of 5-6 that is comparable to the number in **1e** while the piperazine ring was substituted by a small group. Encouragingly, most compounds achieved $K_{puu,brain}$ and $K_{puu,CSF}$ values > 0.5. In particular, the free brain and cerebrospinal fluid AUCs of **1m** were similar to that in blood, indicating its equivalent exposures in brain, CSF and blood.

With the introduction of substituents to the piperazine moiety, several compounds achieved good CNS penetration ($K_{puu,brain}$ and $K_{puu,CSF}$ > 0.5) as well as *in vitro* potency. As the final selection of the compound for progression into pre-clinical testing would be the rat PK profile, potent inhibitors with $K_{puu,brain}$ and $K_{puu,CSF}$ greater than 0.5 were further evaluated in rats (**Table 5**). Overall, these compounds showed good oral bioavailability (>52%) except for compound **1k** (24%). Agent **1m** exhibited the best pharmacokinetic profile with moderate blood clearance at 17 mL/min/kg and the volume of distribution of 5.2 L/kg. The intrinsic clearance (Cl_{int}) of **1m** is 11.4 μL/min/10^6 cells in human hepatocytes and the predicted clearance of the agent in human is 7.7 mL/min/kg by *in vitro-in vivo* extrapolation (IVIVe)[31,32]. Liver blood flow (LBF) method

with blood protein binding correction was applied to generate individual estimates of unbound human hepatic clearance ($CL_{hepatic}$) using available data from each pre-clinical species.[33-35] The predicted human clearance by the LBF method from rat is 8.1 mL/min/kg which is very similar to that derived from IVIVe. Following oral dosing in rats at 2 mg/kg, absorption of **1m** was rapid with blood C_{max} of 0.58 μM achieved at 1.0 h. Subsequently, blood concentrations of **1m** declined mono-exponentially with mean elimination half-life of 4.3 h, which was close to the same parameter obtained from intravenous dosing (4.1 h). The bioavailability following an oral dose in rats was 91%. Given its promising PK properties, CNS penetration and *in vitro* potency, **1m** was selected as the candidate for comprehensive biological profiling.

Table 5. Rat PK Data of Compounds **1i-n** (PO: 2 mg/kg; iv: 1 mg/kg)[a]:

Compounds	**1i**	**1j**	**1k**	**1l**	**1m**	**1n**
Oral $AUC_{0\text{-}24h}$ (nM·h)[b]	1570	2315	789	1037	3803	2948
F (%)[c]	52	84	24	92	91	83
$T_{1/2}$ (h)[d]	0.9	1.3	1.1	1.3	4.1	2.4
CL (mL/min/kg)[e]	28	31	26	55	17	29
V_{ss} (L/kg)[f]	2.0	2.5	1.9	3.2	5.2	2.7

[a]*In vivo* PK was obtained *via* intravenous infusion route (DMSO: 10% Captisol in saline = 1:99) and oral gavage route (1% methylcellulose) in male Wistar Han rats (non-fasted). [b]Area under concentration-time curve from 0-24 hours. [c]Bioavailability (%). [d]Mean elimination half-life, obtained from intravenous infusion. [e]Clearance, obtained from intravenous infusion. [f]Volume of distribution at steady state. All pharmacokinetic parameters were calculated with Phoenix v6.3 (Certara, St Louis, MO, USA).

***In vitro* profile of candidate 1m.** The inhibition of **1m** against EGFR tyrosine kinase (EGFR TK) wild type and mutant enzymes was tested at their corresponding K_m and 2 mM ATP concentrations (**Table 6**). At Km ATP concentrations, the inhibition IC_{50} values were 0.3, 0.2 and 0.2 nM for EGFR TK wild type, L858R mutant and Exon 19Del enzymes, respectively. In cellular EGFR phosphorylation and proliferation studies, PC-9 (Exon 19Del), H3255 (L858R),

and H838 (wild type EGFR) cells were used (see details in Supporting Information). The results are shown in **Table 6**. Compound **1m** was an equally potent inhibitor of cellular phosphorylation or proliferation in EGFR activating mutant cell lines (PC-9 and H3255 cell lines) in a range of 7.0-7.7 nM, suggesting a high level of potency against all these clinically relevant EGFR mutations. In cellular phosphorylation studies, **1m** also demonstrated 9-fold inhibition selectivity in EGFR activating mutant cell lines over EGFR wild type cell lines (H838 cell line). This was consistent with the findings in biochemical assay when ATP concentration was increased from Km to 2mM (the hypothesized cellular ATP concentration), suggesting ATP competitive binding mode of **1m** with its possible differential binding affinities to mutant and wild type EGFRs. Although **1m** showed some activity against pEGFR in H838 cells, as these cells do not rely on activation of EGFR pathway for proliferation, we did not see activity of **1m** on cell proliferation of H838 cells. In contrast, **1m** demonstrated inhibitory effects on both pEGFR pathway and cell proliferation of EGFR mutation derived cells, PC-9 and H3255, suggesting these cells rely on activation of EGFR pathway for proliferation. In order to broadly evaluate the selectivity of the compound, **1m** was screened in a kinase panel and in a secondary pharmacology panel (see details in Supporting Information). Kinase panel, screened at Millipore, comprised of 124 recombinant protein kinases and lipid kinases. The percentage inhibition of **1m** was tested at one single concentration (1 μM) across each of these kinases. At this concentration, **1m** displayed less than 50% inhibition against 115 kinases and greater than 50% inhibition against the other nine kinases including EGFR kinase in the panel. The inhibition of those 8 off targets were 83% for EphB4, 57% for Flt, 58% for Fyn, 62% for KDR, 61% for Lck activated, 74% for Lyn, 69% for Src, and 87% for Yes. Secondary pharmacology panel, performed at Cerep, covered 150 distinct molecular targets. Assays were run in concentration-

response mode. It was found that 147 molecular targets exhibited > 1 μM and 3 targets < 1 μM of IC_{50}s. These active molecular targets with less than 1 μM of IC_{50}s were KDR (156 nM), Src (622 nM), and D2 (797 nM). The results from these panel screening indicated that **1m** was a highly selective compound. Furthermore, **1m** was neither a direct inhibitor (IC_{50} > 50 μM) nor a time dependent inhibitor for CYP1A2, CYP2B6, CYP2C8, CYP2C9, CYP2C19, CYP2D6 and CYP3A4/5 isoforms. This agent exhibited less than 3 fold of mRNA induction for CYP1A2, CYP2B6 and CYP3A4 at the predicted maximum total concentration (0.3 μM) of the compound, suggesting a low enzyme induction liability.[36,37] Also, the candidate showed acceptable hERG inhibition activity with IC_{50} of 13.3 μM in a conventional manual whole-cell patch clamp study.

Table 6. Compound **1m** Activity in Biochemical and Cellular Assays[a]

Biochemical assay						Cellular phosphorylation			Cellular proliferation		
EGFR (Exon 19Del) IC_{50} at Km of ATP (nM) (n = 14)	EGFR (Exon 19Del) IC_{50} at 2 mM of ATP (nM) (n = 5)	EGFR(L858R) IC_{50} at Km of ATP (nM) (n = 65)	EGFR(L858R) IC_{50} at 2 mM of ATP (nM) (n = 10)	EGFR(wt) IC_{50} at Km of ATP (nM) (n = 65)	EGFR(wt) IC_{50} at 2 mM of ATP (nM) (n = 10)	PC-9 (Exon 19Del) pEGFR IC_{50} (nM) (n = 12)	H3255 (L858R) pEGFR IC_{50} (nM) (n = 12)	H838 (wt) pEGFR IC_{50} (nM) (n = 13)	PC-9 (Exon 19Del) GI_{50} (nM) (n = 40)	H3255 (L858R) GI_{50} (nM) (n = 40)	H838 (wt) GI_{50} (nM) (n = 11)
0.2±0.02	2.4±0.3	0.2±0.06	7.6±2.1	0.3±0.04	102±34	7.4±1.3	7.2±1.3	64.5±8.7	7.7±2.6	7.0±1.5	21556±4866

[a]Average value from the n times of repeat tests.

Dog pharmacokinetics. Blood pharmacokinetic parameters of **1m** in male dogs were determined following both a single dose intravenous infusion and oral administration. These data are summarized in **Table 7**. Following the IV dose in dogs, **1m** blood clearance was determined as 14 mL/min/kg and volume of distribution was 6.4 L/kg. Its elimination half life was 6.2 h. Absorption of **1m** was rapid with blood C_{max} (698 nM) occurring between 0.5 h and 1.5 h. The oral bioavailability of **1m** was excellent at 90%.

Table 7. Dog PK Data of **1m**[a]

Dose/route	$AUC_{0\text{-}24h}$ (nM·h)[b]	$T_{1/2}$ (h)[c]	F (%)[d]	T_{max} (h)[e]	C_{max} (nM)[f]	CL (mL/min/kg)[g]	V_{ss} (L/kg)[h]
1 mg/kg/iv	2560	6.2	---	---	---	14	6.4
2 mg/kg/PO	4625	5.5	90.2	0.5-1.5	698	---	---

[a]*In vivo* PK was obtained *via* intravenous infusion route (DMSO: 10% Captisol in saline =1:99) and oral gavage route (1% methylcellulose) in male Beagle dog (Fed). [b]Area under concentration-time curve from 0-24 hours. [c]Mean elimination half-life. [d]Bioavailability (%), calculated with $AUC_{0\text{-}24h}$ and nominal dose. [e]Time to reach maximum concentration. [f]Peak concentration. [g]Clearance. [h]Volume of distribution at steady state. All pharmacokinetic parameters were calculated with Phoenix v6.3 (Certara, St Louis, MO, USA).

Microdosing positron emission tomography (PET) studies. Brain distribution of **1m** in monkey was investigated by microdosing positron emission tomography (PET) to substantiate the PK data in rats.[38] Radio-labeled [^{11}C]-**1m** (0.28 μg, 150 MBq and 0.35 μg, 155 MBq, respectively) was injected into two male cynomolgus monkeys (PET1 and PET2, respectively). The PET distribution volume (V_T) was estimated for the whole brain region using the 2-tissue compartment model.[38] The distribution volume and estimated free brain to plasma partition coefficient ($C_{u,brain}/C_{u,plasma}$) are summarized in **Table 10**. The partition coefficient values (0.50 and 0.53 for PET1 and PET2, respectively) indicated **1m** penetrated extensively into monkey brain. PET images (**Figure 1**) for both monkeys also suggested that the radio-labeled compound was well distributed throughout the brain.

Table 10. Unbound Brain/plasma Ratio for [^{11}C]-**1m** in Cynomolgus Monkey[a]

	Injected mass and radioactivity	V_T (mL•cm–3)	$f_{u,,plasma}$[b]	$f_{u,brain}$[c]	$C_{u,brain}$ / $C_{u,plasma}$
PET1	0.28 μg, 150 MBq	3.0	0.12	0.02	0.50
PET2	0.35 μg, 155 MBq	3.7	0.14	0.02	0.53

[a]PET microdosing studies were performed after a single dose of [^{11}C]-**1m** (phosphate buffered saline, pH 7.4) *via* intravenous bolus route. [b]The unbound fraction in plasma was determined in the PET experiment using ultrafiltration. [c]Data obtained from *in vitro* equilibrium dialysis of rat brain homogenate were used as an estimate of the unbound fraction in monkey brain tissue.[39]

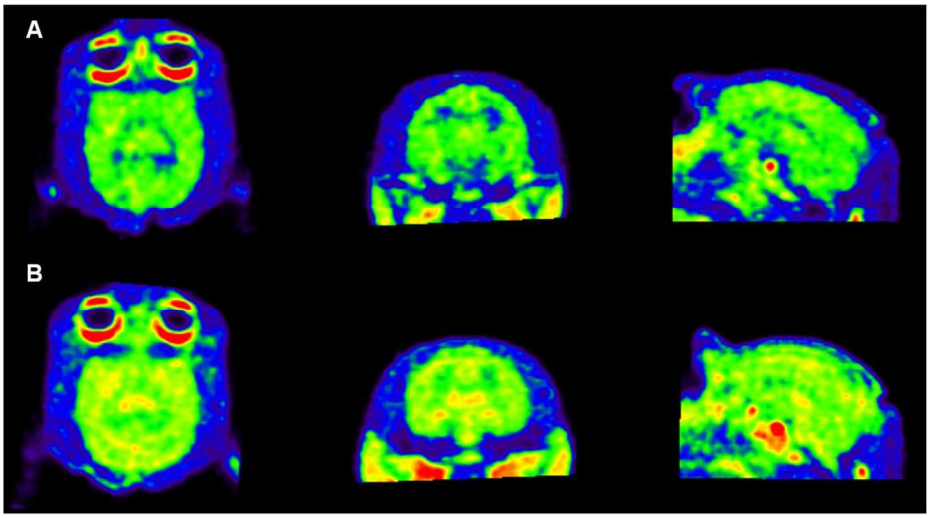

Figure 1. Color-coded PET images showing distribution of radioactivity in the monkey brain following administration of [^{11}C]-**1m**. Horizontal (left panel), coronal (middle panel) and sagittal (right panel) projections for Monkey PET1 (A) and Monkey PET2 (B). Images created from summation images from 5 to 123 minutes and image intensity is normalized for injected radioactivity.

***In vivo* anti-tumor efficacy study.** A brain metastasis model was generated by intracerebral injection of luciferase transfected PC-9 (Exon19Del) cells. Tumor growth was monitored by IVIS Xenogen imaging system. **1m** demonstrated significant dose dependent anti-tumor efficacy (~78% tumor growth inhibition at 7.5 mg/kg qd and tumor regression at 15 mg/kg qd, respectively, 4 weeks after treatment), with <20% body weight loss, while erlotinib had limited effect in this model (**Figure 2A**). At the end of the study, brain tissues were collected for histological assessment. Significantly decreased tumor area was observed by **1m** treatment at the doses of 7.5mg/kg and 15mg/kg (**Figure 2B**). In addition, modulation of pEGFR was detected by a single dose **1m** at 15mg/kg 1h after dosing, which confirmed target engagement by **1m** (**Figure 2C**).

(**A**)

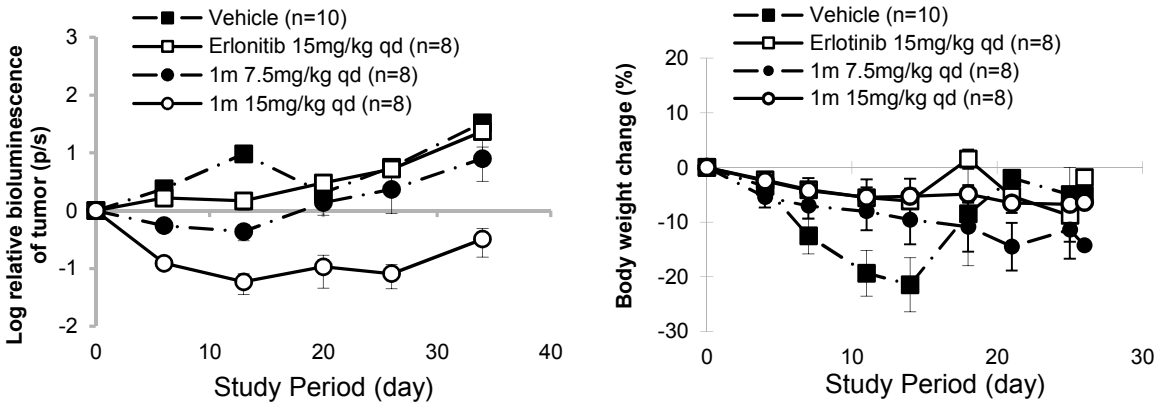

(**B**)

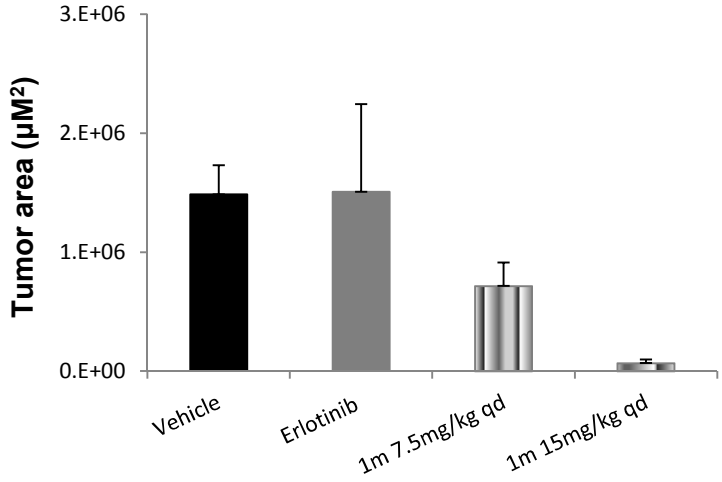

(**C**)

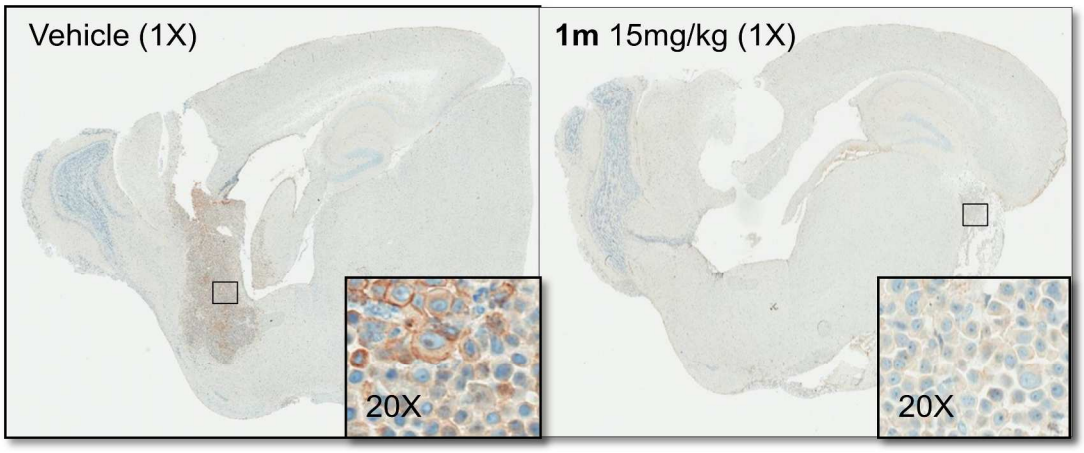

Figure 2. A brain metastasis model was established by injection of luciferase transfected PC-9 cells into the brain parenchyma. Tumor growth was monitored by measuring bioluminescence signals. About 2-3 weeks after cell injection, animals were treated with erlotinib at 15 mg/kg qd,

and **1m** at 7.5 mg/kg qd and 15 mg/kg qd, respectively. **(A)** Significant tumor growth inhibition was observed by **1m** treatment in a dose dependent manner, compared with erlotinib. **(B)** Histological assessment showed dose-dependent reduction of tumor area with **1m** treatment. **(C)** Modulation of pEGFR in tumor tissue was observed by a single dose of **1m** at 15mg/kg 1 h after dosing (at 1X and 20X amplification).

Synthesis **Scheme 3** illustrates the synthesis of key intermediates **6** and **8**. Starting material **3** was conveniently prepared according to literature procedures.[40,41] The reaction of **3** and commercially available **4** was carried out in acetonitrile without the addition of other reagents. The resulting HCl salt of acetate **5** was treated with potassium carbonate in methanol to provide **6**. Another building block, **8**, was readily obtained from commercially available **7** by the reaction with triphosgene in dichloromethane.[42] Crude **6** and **8** were used for the further reactions without purification. Other similar starting materials **18a-h** and **19** were prepared by the same procedure and the crude materials were used directly.

Scheme 3. Synthesis of Intermediate **6** and **8**[a]

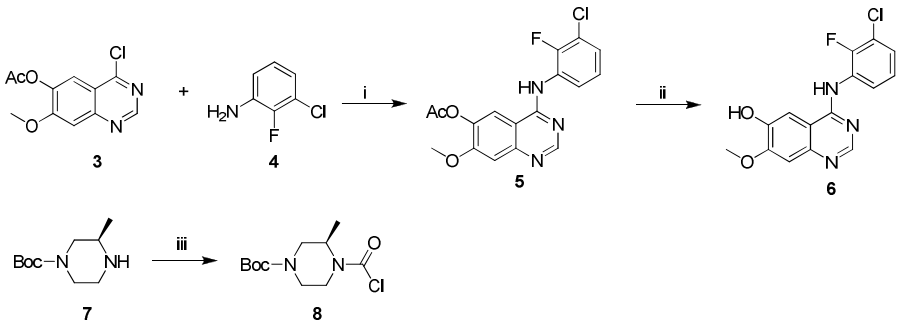

[a]Reagents and conditions: (i) acetonitrile, reflux, 4 h; (ii) potassium carbonate, methanol, 10-15 °C, 2 h; (iii) triphosgene, pyridine, dichloromethane, 0 °C to rt.

Scheme 4 describes the synthesis of **1a** and **1c**. Triflate **9**, prepared from **6**, was conveniently converted to **1c** under conditions described in the literature.[43] Heck reaction of **9** with methyl acrylate delivered **10** which was subjected to ozonolysis to give aldehyde **11**. This agent was then reacted with morpholine under reductive condition to afford desired compound **1a**.

Scheme 5 depicts the synthetic route of **1b** and **2**. Triflate **13**, prepared from commercially available **12** under typical conditions, reacted with morpholine to provide **14**. After reduction of **14**, the resulting **15** was converted into a quinazoline derivative **16** by using formamidine acetate in ethanol. The preparation of reactive intermediate **17** from **16** was accomplished with oxalyl chloride in chloroform at an elevated temperature. With this key material, **1b** and **2** were synthesized by substitution reaction without addition of other basic reagents.

Scheme 4. Synthesis of **1a** and **1c**[a]

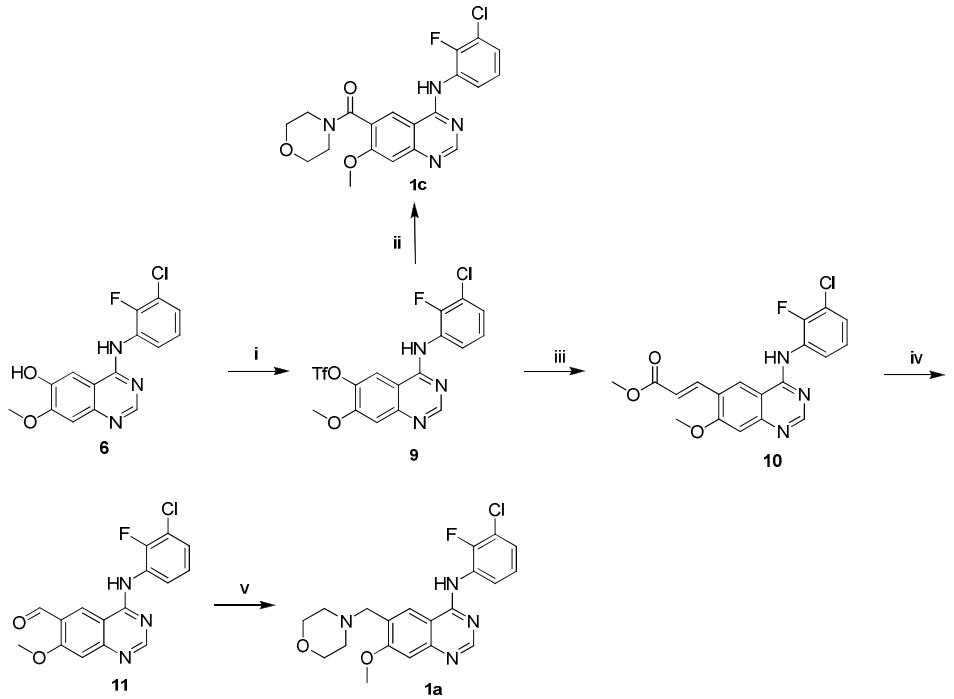

[a]Reagents and conditions: (i) Tf_2O, pyridine, 5 °C to rt; (ii) CO, $Pd(OAc)_2$, dppf, morpholine, 70 °C, overnight; (iii) methyl acrylate, $Pd(OAc)_2$, Et_3N, dppf, Bu_4NBr, DMF, 80 °C, overnight; (iv) O_3, CH_2Cl_2, -78 °C then $(CH_3)_2S$, -78 °C to rt; (v) morpholine, $NaBH_3CN$, acetic acid, rt.

Scheme 5. Synthesis of **1b** and **2**[a]

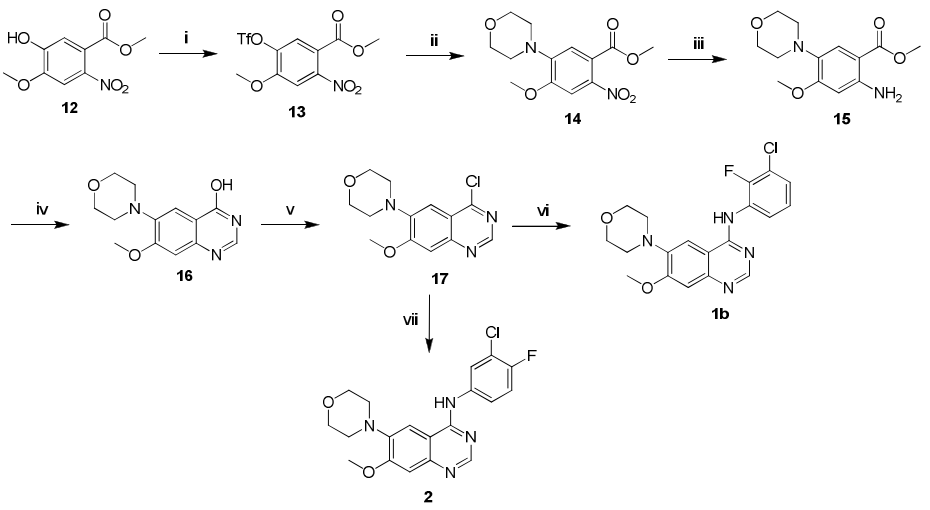

[a]Reagents and conditions: (i) Tf_2O, pyridine, CH_2Cl_2, 0 °C to rt, 16 h; (ii) morpholine, CH_3CN, reflux, overnight; (iii) Fe, NH_4Cl, CH_3OH, H_2O, 80 °C, 4 h; (iv) formamidine acetate salt, C_2H_5OH, reflux, overnight; (v) oxalyl chloride, $CHCl_3$, DMF, 60 °C, 2 h; (vi) 3-chloro-2-fluoroaniline, CH_3CN, reflux, 18 h; (vii) 3-chloro-4-fluoroaniline, CH_3CN, reflux, 2 days.

Scheme 6. General Synthesis of Compounds **1d-h**, **1k-l,** and **1n**[a]

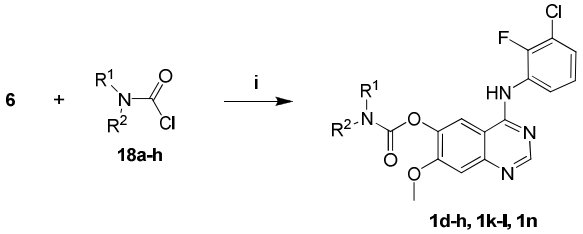

[a]Reagents and conditions: (i) $(C_2H_5)_3N$ or K_2CO_3, CH_2Cl_2 or DMF, rt.

Scheme 7. Synthesis of **1i** and **1j**[a]

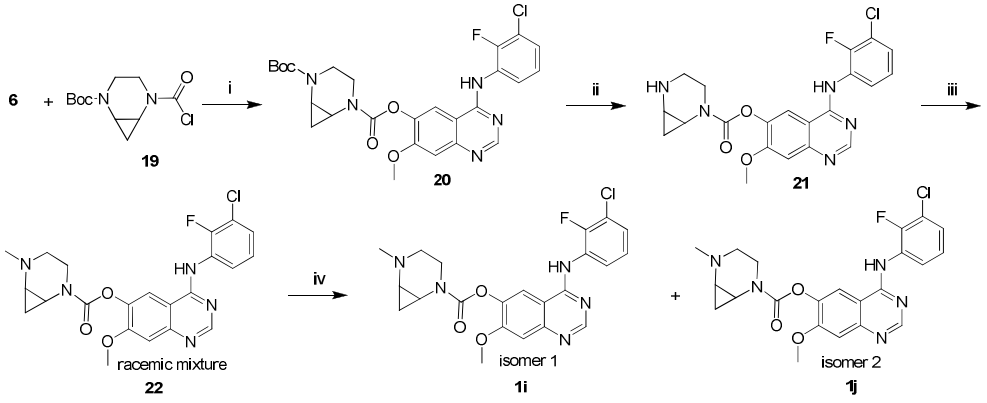

[a]Reagents and conditions: (i) K_2CO_3, DMF, rt, overnight; (ii) HCl, 1,4-dioxane, ethyl acetate, rt, 1 h; (iii) paraformaldehyde, $NaBH_3CN$, CH_3CO_2H, methanol, rt, overnight; (iv) chiral SFC.

Scheme 8. Synthesis of **1m**[a]

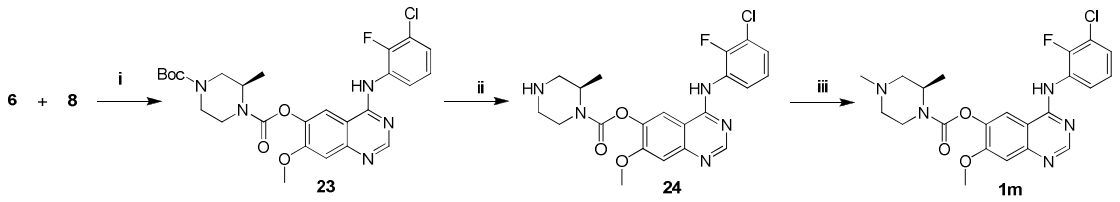

[a]Conditions and reagents: (i) potassium carbonate, DMF, rt; (ii) HCl in dioxane, methanol, rt; (iii) paraformaldehyde, sodium cyanoborohydride, methanol, rt.

The syntheses of compounds **1d-h**, **1k-l**, and **1n** are illustrated in **Scheme 6**. The carbamate formation was carried out in basic media at room temperature. Carbamate **20** was prepared (**Scheme 7**) in a similar manner. The subsequent de-protection of **20** and reductive methylation of **21** provided a racemic mixture (**22**). The resolution of this mixture by chiral SFC technology delivered two optically pure isomers **1i** and **1j**. The preparation of compound **1m** from a chiral staring material (**8**) by a similar synthetic route is outlined in **Scheme 8**.

▪ CONCLUSION

By correctly balancing physicochemical properties, such as permeability, solubility and efflux ratio, we were able to identify compound **1a**. This early lead has significantly improved CNS penetration without compromising the *in vitro* potency. Replacement of methylene group present in **1a** by carbamate linker led to compound **1e**. This compound significantly improved metabolic stability. The terminal basic nitrogen in **1e** was found to be an essential element to achieve good exposures in both brain and blood. By incorporating a methyl group into the piperazine moiety, we further improved PK properties of **1e**, leading to successful discovery of clinical candidate **1m**. **1m** exhibited excellent free compound distribution in brain, CSF, and blood. The extensive *in vitro* evaluation, including biochemical, cellular, and panel screening, indicates that this agent is highly potent against EGFR activating mutants and highly selective towards these targets. Importantly, **1m** showed tumor regression in the mouse model with brain metastasis. The promising data package for **1m** strongly supported its selection as a drug

candidate for development. The results from additional *in vivo* studies are due to be published separately.

▪ EXPERIMENTAL SECTION

***In vivo* animal model.** PC-9 cells (EGFR Exon19 deletion) were cultured with RPMI-1640 medium supplemented with 10% fetal bovine serum (FBS) at 37 °C. In order to monitor tumor growth in the brain, PC-9 cells were stably transfected with pGL4.50[luc2/CMV/Hygro] vector containing luciferase, and the bioluminescence signals were measured by a Xenogen imaging system.[44] A brain metastasis model was established by intracerebral (ICB) injection of PC-9_Luc cells using the method by Lal with modifications.[45] In brief, after a sagittal incision over the parieto-occipital bone, a hole was punctured on the skull at 2.5 mm to the right of the bregma and 1 mm anterior to the coronal suture. Then the syringe was placed perpendicular to the skull through the hole and placed 3 mm deep below the skull surface, and the PC-9_Luc cell suspension was slowly injected. After injection, the sterile bone gel was applied to the hole, the scalp was pulled back to cover the skull and the wound was closed. The mouse was gently put on a heating pad to recover, and closely monitored after surgery. All *in vivo* studies were approved by the Institutional Animal Care and Use Committee (IACUC) before the experiments were started.

Xenograft tissues were obtained from PC-9 model after treatment with **1m** for assessment of histology and pEGFR modulation. Samples were harvested following formalin fixation and paraffin embedding (FFPE) for further study. pEGFR(Tyr1068) (DAKO X9003) IHC was performed on 3μm FFPE sections using a Ventana automation (Roche) for staining.

Chemistry, Materials, and General Methods. Unless otherwise noted, all reagents and solvents were obtained from commercial suppliers such as Aldrich, Sigma, Fluka, Acros, EMD

Sciences, etc., and used without further purification. Dry organic solvents (dichloromethane, acetonitrile, DMF, etc.) were purchased from Aldrich packaged under nitrogen in Sure/Seal bottles. All reactions involving air or moisture sensitive reagents were performed under a nitrogen or argon atmosphere. Silica gel chromatography was performed using prepacked silica gel cartridges (Biotage or RediSep). ^{1}H NMR spectra were recorded on a Bruker AV 400 MHz, Bruker AV Ⅱ 400 MHz, Bruker AV Ⅲ 400 MHz, or a Varian 400 MHz spectrometer at ambient temperature. Chemical shifts are reported in parts per million (ppm, δ units). Data are reported as follows: chemical shift, multiplicity (s = singlet, d = doublet, t = triplet, q = quartet, br = broad, m = multiplet), coupling constants, and number of protons. Reactions were monitored using LCMS (Shimadzu 20A) with UV detection at 220 & 254 nm and a low resonance electrospray mode (ESI). All final compounds were purified to > 95% purity, as determined by LCMS (4 min). LCMS (4 min) methods used the following: Shimadzu 20A spectrometer, Xtimate C18 2.1 x 30 mm, 3 μm at 50 °C with a 0.8 mL/min flow rate; solvent A of 1.5 mL TFA in 4 L water, solvent B of 0.75 mL TFA in 4 L acetonitrile; 0.0–3.0 min, 10% B; 3.0–3.5 min, 80% B; 3.51–4.0 min, 10% B. Flow from UV detector was split (1:2) to the MS detector, which was configured with ESI as ionizable source. All high resolution mass spectrometry (HRMS) data were acquired on an Agilent 1100 Series (LC/MSD TOF G3251) operated in positive electrospray ionization mode. The mobile phase: 0.1% TFA in water (solvent A) and 0.1% TFA in acetonitrile (solvent B), using the elution gradient 10%-80% (solvent B) over 2 minutes and holding at 80% for 1 minute, then back to 10% and holding at 10% for 1 minute at a flow rate of 1 mL/minute. Nebulization Gas: nitrogen; Time of Flight mass spectrometer with ESI source; Positive ion mode; Drying gas (N_2) flow: 12 l/min; nebulizer pressure: 20 psi, 350 Centigrade; Capillary voltage: 3000V. The fragmentor voltage: 50V.

4-(3-Chloro-2-fluorophenylamino)-7-methoxyquinazolin-6-yl acetate (5). To a suspension of 4-chloro-7-methoxyquinazolin-6-yl acetate (**3)** (100 g, 396 mmol) in acetonitrile (4 L) was added 3-chloro-2-fluoroaniline (**4**) (57.8 g, 396.8 mmol). The reaction mixture was heated to reflux for 4 h with stirring before being cooled to room temperature. After filtration, the cake was washed with acetonitrile (1 L) and dried *in vacuo* to afford the HCl salt of **5** (143.3 g, 91%) as a white solid. ^{1}H NMR (400 MHz, DMSO-d_6): δ 11.64 (s, 1H), 8.87 (s, 1H), 8.68 (s, 1H), 7.67-7.62 (m, 1H), 7.52 (s, 2H), 7.39-7.33 (m, 1H), 4.01 (s, 3H), 2.39 (s, 3H). LCMS (ESI) *m*/*z* calculated for $C_{17}H_{13}ClFN_3O_3 + H^+$ [M+H$^+$]: 362.1. Found: 361.8.

4-(3-Chloro-2-fluorophenylamino)-7-methoxyquinazolin-6-ol (6). Potassium carbonate (114.0 g, 826 mmol) was added to a solution of HCl salt of **5** (150.0 g, 377 mmol) in methanol (800 ml). The reaction mixture was stirred at 10-15 °C for 2 h. After filtration, the solid was rinsed with methanol (120 mL). The filtrate was concentrated *in vacuo* to a residue (~300 g) and treated with methyl *tert*-butyl ether (800 mL). The resulting mixture was filtered. The solid was dried at 40-45 °C to afford a potassium salt of compound **6** (132.0 g, 98%). ^{1}H NMR (400 MHz, DMSO-d_6): δ 7.97 (s, 1H), 7.61-7.57 (m,1H), 7.24-7.11 (m, 2H), 7.29-7.25 (m,1H), 6.89 (s,1H), 6.79 (s, 1H), 3.77 (s, 3H). LCMS (ESI) *m*/*z* calculated for $C_{15}H_{11}ClFN_3O_2 + H^+$ [M+H$^+$]: 320.1. Found: 319.9.

(*R*)-*tert*-Butyl 4-(chlorocarbonyl)-3-methylpiperazine-1-carboxylate (8). Pyridine (18 g, 225 mmol) was added drop-wise to a mixture of triphosgene (23 g, 75 mmol) in dry dichloromethane (250 mL) followed by (*R*)-4-Boc-2-methylpiperazine (**7**) (15 g, 75 mmol) at 0 °C under nitrogen. The reaction mixture was stirred overnight at room temperature and concentrated to afford **8** as a yellow solid, which was used without further purification.

4-(3-Chloro-2-fluorophenylamino)-7-methoxyquinazolin-6-yl trifluoromethanesulfonate (9). Pyridine (5 g, 62.4 mmol) was added to a solution of **6** (5 g, 15.6 mmol) in dichloromethane (60 mL) followed by the addition of trifluoromethanesulfonic anhydride (13.2 g, 46.8 mmol) dropwise at 5 °C. The reaction mixture was warmed to room temperature and stirred at that temperature overnight. The mixture was treated with water and separated. The organic layer was dried over sodium sulfate and concentrated. The residue was purified by chromatography using silica gel column and eluting with ethyl acetate in petroleum (1:3) to afford **9** (5.2 g, 11.53 mmol, 74%) as a yellow solid. ^{1}H NMR (400 MHz, $CDCl_3$): δ 8.81 (s, 1H), 8.42-8.39 (m, , 1H), 7.76 (s, 1H), 7.46 (s, 1H), 7.39 (s, 1H), 7.24-7.18 (m, 2H), 4.10 (s, 3H). LCMS (ESI) *m*/*z* calculated for $C_{16}H_{10}ClF_4N_3O_4S + H^+$ [M+H$^+$]: 452.0. Found: 451.8.

(*E*)-Methyl 3-(4-(3-chloro-2-fluorophenylamino)-7-methoxyquinazolin-6-yl)acrylate (10). Methyl acrylate (2.21 g, 25.7 mmol), $Pd(OAc)_2$ (287 mg, 1.28 mmol), 1,1'-bis(diphenylphosphino)ferrocene (710 mg, 1.28 mmol), Bu_4NBr (4.13 g, 12.8 mmol) and Et_3N (2.6 g, 25.7 mmol) were added to a solution of **9** (5.8 g, 12.8 mmol) in DMF (200 mL). The reaction mixture was degassed and refilled with nitrogen three times. The mixture was stirred at 80 °C overnight, cooled to room temperature, and treated with ethyl acetate (500 mL) and water (600 mL). After separation, the aqueous layer was extracted with ethyl acetate three times. The combined extracts were washed with brine, dried over sodium sulfate, and concentrated. The residue was purified by flash chromatography eluting with ethyl acetate in petroleum (1:2) to afford **10** (4 g, 10.3 mmol, 80%). ^{1}H NMR (400 MHz, $CDCl_3$): δ 8.76 (s, 1H), 8.48-8.44 (m, 1H), 8.07-7.03 (m, 2H), 7.72 (s, 1H), 7.30 (s, 1H), 7.23-7.16 (m, 2H), 6.74 (d, *J* = 16.4 Hz, 1H), 4.06 (s, 3H), 3.86 (s, 3H). LCMS (ESI) *m*/*z* calculated for $C_{19}H_{15}ClFN_3O_3 + H^+$ [M+H$^+$]: 388.1. Found: 387.9.

4-(3-Chloro-2-fluorophenylamino)-7-methoxyquinazoline-6-carbaldehyde (11). A solution of **10** (4 g, 10.3 mmol) in dichloromethane (100 mL) was cooled with dry-ice bath and ozone gas was bubbled into the solution for 15 min. The nitrogen was bubbled into the mixture to remove O_3. After addition of methyl sulfide (3.2 g, 51.9 mmol), the mixture was warmed to room temperature and stirred at that temperature for 30 min. The solvent was removed *in vacuo* and the residue was purified by flash chromatography eluting with petroleum in ethyl acetate (2: 1) to afford **11** (1.3 g, 38% yield) as yellow solid. ^{1}H NMR (400 MHz, $CDCl_3$): δ 10.58 (s, 1H), 8.79 (s, 1H), 8.54 (s, 1H), 8.34 (t, *J* = 7.2 Hz, 1H), 7.50 (s, 1H), 7.25-7.18 (m, 2H), 4.12 (s, 3H). LCMS (ESI) *m*/*z* calculated for $C_{16}H_{11}ClFN_3O_2 + H^+$ [M+H$^+$]: 332.1. Found: 332.1.

N-(3-Chloro-2-fluorophenyl)-7-methoxy-6-(morpholinomethyl)quinazolin-4-amine (1a). Morpholine (420 mg, 4.82 mmol) and acetic acid (289 mg, 4.82 mmol) were added to a solution of **11** (800 mg, 2.41 mmol) in methanol (10 mL). The reaction mixture was stirred at room temperature for 30 min and $NaBH_3CN$ (227 mg, 3.61 mmol) was added. The resulting mixture was stirred at room temperature for additional 1 h and concentrated. The residue was purified by reverse phase preparative HPLC using Agella Venusil ASB C18 150 x 21 mm, 5 μm column and eluting with a gradient of 5-35% acetonitrile in water containing 0.05% HCl to afford HCl salt of **1a** (575.2 mg, 1.31 mmol, 54%). ^{1}H NMR (400 MHz, CD_3OD): δ 8.87 (s, 1H), 8.81 (s, 1H), 7.59-7.53 (m, 2H), 7.39 (s, 1H), 7.35-3.31 (m, 1H), 4.62 (s, 2H), 4.19 (s, 3H), 4.07 (d, *J* = 12.8 Hz, 2H), 3.91 (t, *J* = 12.0 Hz, 2H), 3.54 (d, *J* = 12.0 Hz, 2H), 3.43-3.37 (m, 2H). ^{13}C NMR (101 MHz, CD_3OD): δ 166.1, 162.4, 153.5, 153.0, 143.6, 132.2, 131.6, ,128.3, 126.9, 126.3, 123.1, 122.6, 108.2, 100.9, 65.0, 58.2, 56.4, 53.6. HRMS(ESI): *m*/*z* calculated for $C_{20}H_{20}ClFN_4O_2 + H^+$ [M + H$^+$]: 403.1337. Found 403.1302

Methyl 4-methoxy-2-nitro-5-(trifluoromethylsulfonyloxy)benzoate (13). Pyridine (8.7 g, 110 mmol) was added to a solution of methyl 5-hydroxy-4-methoxy-2-nitrobenzoate (5 g, 22 mmol) in dichloromethane (50 mL). The reaction mixture was cooled to 0 °C with ice-water, and then trifluoromethanesulfonic anhydride (12.4 g, 44 mmol) was added slowly to maintain the internal temperature below 10 °C. The reaction mixture was slowly warmed to room temperature and stirred at that temperature for 16 h. Water (100 mL) was then added and the organic layer was separated. The aqueous layer was extracted with dichloromethane (3 x 100 mL). The combined organic layers were washed with citric acid solution (2 x 100 mL) and brine. The organic solution was dried over sodium sulfate and concentrated to afford **13** (5.9 g, 75%) as a yellow solid. This material was used for the next reaction without purification. ^{1}H NMR (400 MHz, $CDCl_3$): δ 7.71 (s, 1H), 7.41 (s, 1H), 4.05 (s, 3H), 3.91 (s, 3H).

Methyl 4-methoxy-5-morpholino-2-nitrobenzoate (14). Morpholine (0.73 g, 7.35 mmol) was added to a solution of **13** (1 g, 2.78 mmol) in acetonitrile (20 mL). The reaction mixture was refluxed overnight prior to the addition of a second batch of morpholine (0.5 g, 5.73 mmol). The reaction mixture was refluxed for an additional 3 h and cooled to room temperature. The solvent was evaporated *in vacuo* and the residue was purified by flash chromatography eluting with ethyl acetate in petroleum (1:3) to afford **14** (800 mg, 2.7 mmol, 97%). ^{1}H NMR (400 MHz, $CDCl_3$): δ 7.48 (s, 1H), 7.02 (s, 1H), 3.96 (s, 3H), 3.90 (s, 3H), 3.87 (t, J = 4.8 Hz, 4H), 3.21 (t, J = 4.8 Hz, 4H).

Methyl 2-amino-4-methoxy-5-morpholinobenzoate (15). Water (5 mL), ammonium chloride (1.44 g, 27 mmol) and iron powder (753 mg, 13.5 mmol) were added to a solution of **14** (800 mg, 2.7 mmol) in methanol (15 mL). The suspension was heated to 60 °C for 4 h and cooled to room temperature. The mixture was filtered. The filtration cake was rinsed with dichloromethane.

After separation of the filtrate, the aqueous layer was extracted with dichloromethane (2 x 50 mL). The combined extracts were dried over sodium sulfate and concentrated to afford **15** (720 mg, 2.7 mmol, 100%) as a yellow solid. This product was used for the next step without purification.

7-Methoxy-6-morpholinoquinazolin-4-ol (16). Formamidine acetate salt (563 mg, 5.4 mmol) was added to a solution of **15** (720 mg, 2.7 mmol) in ethanol (20 mL). The reaction mixture was refluxed overnight and cooled to room temperature. The solvent was evaporated *in vacuo* and the residue was suspended with water (10 mL). The solid was collected by filtration and dried *in vacuo* to afford **16** (400 mg, 1.53 mmol, 57%) as a white solid. ^{1}H NMR (400 MHz, DMSO-d_6): δ 12.10 (br, 1H), 7.97 (s, 1H), 7.44 (s, 1H), 7.12 (s, 1H), 3.93 (s, 3H), 3.76 (t, J = 4.4 Hz, 4H), 3.03 (t, J = 4.4 Hz, 4H). LCMS (ESI) m/z calculated for $C_{13}H_{15}N_3O_3 + H^+$ [M+H$^+$]: 262.1. Found: 262.1.

4-(4-Chloro-7-methoxyquinazolin-6-yl)morpholine (17). Three drops of DMF was added to a suspension of **16** (600 mg, 2.3 mmol) in chloroform (10 mL) followed by the dropwise addition of oxalyl chloride (870 mg, 6.9 mmol). The reaction mixture was stirred at 80 °C for 2 h and cooled to room temperature. The solvent was evaporated *in vacuo* to afford **17** (644 mg, 100%) as a brown solid, which was used for the next step directly. LCMS (ESI) m/z calculated for $C_{13}H_{14}ClN_3O_2 + H^+$ [M+H$^+$]: 280.1. Found: 279.8.

N-(3-Chloro-2-fluorophenyl)-7-methoxy-6-morpholinoquinazolin-4-amine (1b). 3-Chloro-2-fluoroaniline (670 mg, 4.6 mmol) was added to a suspension of **17** (644 mg, 2.3 mmol) in acetonitrile (10 mL). The reaction mixture was refluxed for 18 h and cooled to room temperature. The solvent was evaporated *in vacuo* and the residue was purified by reverse phase preparative HPLC using YMC-pack ODS-AQ 150 x 30 mm, 5 μm column and eluting with a

gradient of 35-65% acetonitrile (containing 0.05% ammonia) in water to afford **1b** (446.6 mg, 1.15 mmol, 50%) as a white solid. ^{1}H NMR (400 MHz, CD_3OD): δ 8.36 (s, 1H), 7.72 (s, 1H), 7.58-7.54 (m, 1H), 7.44-7.41 (m, 1H), 7.25 (d, *J* = 9.6 Hz, 1H), 7.22 (s, 1H), 4.05 (s, 3H), 3.93-3.90 (m, 4H), 3.23-3.21 (m, 4H). HRMS(ESI): *m*/*z* calculated for $C_{19}H_{18}ClFN_4O_2 + H^+$ [M + H^+]: 389.1181. Found: 389.1186.

N-(3-Chloro-4-fluorophenyl)-7-methoxy-6-morpholinoquinazolin-4-amine (2). 3-Chloro-4-fluoroaniline (166 mg, 1.14 mmol) was added to a suspension of **17** (160 mg, 0.57 mmol) in acetonitrile (3 mL). The reaction mixture was refluxed for 2 days and cooled to room temperature. The mixture was treated with water, neutralized with sodium carbonate solution, and extracted with ethyl acetate (3 x 100 mL). The combined organic layers were dried over sodium sulfate and concentrated. The residue was purified by reverse phase preparative HPLC using Agella Venusil ASB C18 150 x 25 mm, 5 μm column and eluting with a gradient of 9-79% acetonitrile (containing 0.05% HCl) in water to afford HCl salt of **2** (110.8 mg, 0.26 mmol, 49%) as a white solid. ^{1}H NMR (400 MHz, CD_3OD): δ 8.72 (s, 1H), 7.96-7.94 (m, 2H), 7.69-7.66 (m, 1H), 7.39 (t, *J* = 8.8 Hz, 1H), 7.26 (s, 1H), 4.13 (s, 3H), 3.93-3.91 (m, 4H), 3.230-3.28 (m, 4H). ^{13}C NMR (101 MHz, CD_3OD): δ 162.0, 160.4, 156.6, 149.8, 145.7, 138.0, 135.2, 128.4, 126.4, 121.9, 118.1, 112.0, 109.2, 100.6, 68.0, 57.5, 52.5. HRMS(ESI): *m*/*z* calculated for $C_{19}H_{18}ClFN_4O_2 + H^+$ [M + H^+]: 389.1181. Found: 389.1205.

(4-(3-Chloro-2-fluorophenylamino)-7-methoxyquinazolin-6-yl)(morpholino)methanone (1c). $Pd(OAc)_2$ (10 mg, 0.044 mmol) and 1,1'-bis(diphenylphosphino)ferrocene (24 mg, 0.044 mmol) were added to a solution of **9** (200 mg, 0.44 mmol) in morpholine (10 mL). The reaction mixture was stirred at 70 °C under carbon monoxide atmosphere (45 psi) overnight. After being cooled to room temperature, the solvent was evaporated *in vacuo*. The residue was purified by

reverse phase preparative HPLC using Phenomenex Gemini C18 200 x 25 mm, 10 μm column and eluting with a gradient of 30-50% acetonitrile in water to afford **1c** (70.6 mg, 0.17 mmol, 39%). ^{1}H NMR (400 MHz, CD_3OD): δ 8.48 (s, 1H), 8.30 (s, 1H), 7.59—7.55 (m, 1H), 7.45-7.42 (m, 1H), 7.31 (s, 1H), 7.27-7.23 (m, 1H), 4.06 (s, 3H), 3.84-3.77 (m, 4H), 3.69-3.64 (m, 2H), 3.37-3.34 (m, 2H). ^{13}C NMR (101 MHz, CD_3OD): δ 168.6, 161.1, 160.5, 157.1, 155.8, 153.5, 129.4, 128.4, 127.9, 125.9, 124.4, 122.8, 122.7, 110.7, 107.3, 68.1, 67.8, 57.0, 43.8. HRMS(ESI): *m/z* calculated for $C_{20}H_{18}ClFN_4O_3 + H^+$ [M + H^+]: 417.1130. Found: 417.1144.

4-(3-Chloro-2-fluorophenylamino)-7-methoxyquinazolin-6-yl morpholine-4-carboxylate (1d). Morpholine-4-carbonyl chloride (**18a**) (250 mg, ~1.7 mmol) was added to a solution of **6** (500 mg, 1.4 mmol) and Et_3N (285 mg, 2.8 mmol) in anhydrous dichloromethane (20 mL). The reaction mixture was stirred at 25 °C overnight and concentrated under reduced pressure. The residue was purified by reverse phase preparative HPLC using Synergi C18 200 x 25mm, 10 μm column and eluting with 0-41% acetonitrile in water to give **1d** (272 mg, 0.63 mmol, 45%) as a yellow solid. ^{1}H NMR (400 MHz, CD_3OD): δ 8.46 (s, 1H), 8.11 (s, 1H), 7.62-7.58 (m, 1H), 7.43-7.40 (m, 1H), 7.31 (s, 1H), 7.26-7.22 (m, 1H), 4.03 (s, 3H), 3.78 (br, 6H), 3.58 (br, 2H). ^{13}C NMR (101 MHz, CD_3OD): δ 160.1, 158.5, 156.0, 155.1, 151.0, 142.2, 129.2, 129.0, 127.8, 125.9, 122.8, 122.6, 117.4, 110.2, 108.4, 67.7, 57.1, 46.7. HRMS (ESI): m/z calculated for $C_{20}H_{18}ClFN_4O_4 + H^+$ [M + H^+]: 433.1079. Found: 433.1106.

4-(3-Chloro-2-fluorophenylamino)-7-methoxyquinazolin-6-yl 4-methylpiperazine-1-carboxylate (1e). 4-methylpiperazine-1-carbonyl chloride (**18b**) (19.9 g, ~122.3 mmol) and potassium carbonate (27.5 g, 196 mmol) were added to a solution of **6** (15.64 g, 48.9 mmol) in DMF (270 mL). The reaction mixture was stirred at room temperature for 60 h before being treated with water (100 mL) and extracted with CH_2Cl_2 (3 x 500 mL). The combined organic

layers were washed with brine, dried over Na_2SO_4, and concentrated under vacuum. The residue was purified by column chromatography on silica gel eluting with methanol in ethyl acetate (1:10) to afford **1e** (3.586 g, 8.06 mmol, 16%) as a yellow solid. ^{1}H NMR (400 MHz, CD_3OD): δ 8.45 (s, 1H), 8.10 (s, 1H), 7.61-7.58 (m, 1H), 7.43-7.40 (m, 1H), 7.30 (s, 1H), 7.26-7.23 (m, 1H), 4.03 (s, 3H), 3.80 (br, 2H), 3.61 (br, 2H), 2.55 (br, 4H), 2.39 (s, 3H). ^{13}C NMR (101 MHz, CD_3OD): δ 160.0, 158.5, 156.0, 155.0, 153.2, 151.0, 142.2, 129.1, 127.7, 125.9, 125.8, 122.8, 117.4, 110.2, 108.3, 57.1, 55.8, 46.3, 45.7. HRMS(ESI): *m*/*z* calculated for $C_{21}H_{21}ClFN_5O_3 + H^+$ [M + H^+]: 446.1395. Found: 446.1421.

(*R*)-4-(3-Chloro-2-fluorophenylamino)-7-methoxyquinazolin-6-yl 3-(dimethylamino)pyrrolidine-1-carboxylate (1f). Quinazolin-6-ol derivative **6** (4 g, 11 mmol) and potassium carbonate (4.5 g, 33 mmol) were added to a solution of (*R*)-3-(dimethylamino)pyrrolidine-1-carbonyl chloride (**18c**) (5 g, ~22 mmol) in DMF (100 mL). The resulting solution was stirred at room temperature overnight and poured into water (500 mL). After extraction with dichloromethane (3 x 300 mL), the combined organic layers were dried and concentrated. The residue was purified by reverse phase preparative HPLC using Phenomenex Gemini C18 200 x 25 mm, 10 μm column and eluting with a gradient of 25-55% acetonitrile (containing 0.05% ammonia) in water to afford **1f** (2100 mg). The free base was treated with 1N HCl (5 mL) solution and lyophilized to afford HCl salt of **1f** (2231 mg, 4.50 mmol, 20%) as a yellow solid. ^{1}H NMR (400 MHz, CD_3OD): δ 8.58 (s, 1H), 8.24 (d, J = 5.2, 1H), 7.60-7.56 (m, 1H), 7.50-7.46 (m, 1H), 7.35 (s, 1H), 7.30-7.25 (m, 1H), 4.27-4.22 (m, 1H), 4.14-3.91 (m, 2H), 4.05 (s, 3H), 3.89-3.55 (m, 2H), 3.02 (s, 3H), 3.01 (s, 3H), 2.64-2.55 (m, 1H), 2.42-2.27 (m, 1H). HRMS (ESI): *m*/*z* calculated for $C_{22}H_{23}ClFN_5O_3 + H^+$ [M + H^+]: 460.1552. Found: 460.1576.

(S)-4-(3-Chloro-2-fluorophenylamino)-7-methoxyquinazolin-6-yl 3-(dimethylamino)pyrrolidine-1-carboxylate (1g). Quinazolin-6-ol analog **6** (1.8 g, 5 mmol) and potassium carbonate (2 g, 15 mmol) were added to a solution of (*S*)-3-(dimethylamino)pyrrolidine-1-carbonyl chloride (**18d**) (crude, ~10 mmol) in DMF (100 mL). The reaction mixture was stirred at room temperature overnight and poured into water (500 mL). After extraction with dichloromethane (3 x 300 mL), the combined organic layers were dried and concentrated. The residure was purified by reverse phase preparative HPLC using Phenomenex Gemini C18 200 x 25 mm, 10 μm column and eluting with a gradient of 20-50% acetonitrile (containing 0.05% ammonia) in water to afford **1g** (530 mg). The free base was treated with 1N HCl (1.3 mL) solution and lyophilized to give HCl salt (558.7 mg, 1.12 mmol, 22%) as a yellow solid. ^{1}H NMR (400 MHz, CD_3OD): δ 8.54 (s, 1H), 8.22 (s, J = 5.6, 1H), 7.58-7.56 (m, 1H), 7.46-7.30 (m, 1H), 7.34 (s, 1H), 7.28-7.26 (m, 1H), 4.26-3.90 (m, 3H), 4.04 (s, 3H), 3.85-3.54 (m, 2H), 3.01 (s, 3H), 3.00 (s, 3H), 2.66-2.52 (m, 1H), 2.40-2.31 (m, 1H). HRMS (ESI): *m*/*z* calculated for $C_{22}H_{23}ClFN_5O_3 + H^+$ [M + H^+]: 460.1552. Found: 460.1549.

(1*S*,4*S*)4-(3-Chloro-2-fluorophenylamino)-7-methoxyquinazolin-6-yl 5-methyl-2,5-diazabicyclo[2.2.1]heptane-2-carboxylate (1h). A mixture of **6** (1.5 g, 4.69 mmol), (1*S*,4*S*)-5-methyl-2,5-diazabicyclo[2.2.1]heptane-2-carbonyl chloride (**18e**) (crude, ~13.37 mmol), and triethylamine (950 mg, 9.38 mmol) in dichloromethane (20 mL) was stirred at room temperature overnight. After filtration, the filtrate was concentrated and the residue was purified by reverse phase preparative HPLC using Synergi 250 x 77 mm, 10 μm column and eluting with a gradient of 5-40% acetonitrile (containing 0.05% HCl) in water to afford HCl salt of **1h** as a white solid (836.5 mg, 1.69 mmol, 36%). ^{1}H NMR (400 MHz, $CDCl_3$): δ 8.75 (s ,1H), 8.51-8.46 (m, 1H), 7.68 (s, 1H), 7.50 (s, 1H), 7.33 (s, 1H), 7.18-7.16 (m, 2H), 4.63-4.50 (m, 1H), 3.99 (s, 3H), 3.93-

3.75 (m, 1H), 3.56-3.35 (m, 2H), 3.08-2.85 (m, 2H), 2.55-2.53 (m, 3H), 2.03-1.87 (m, 2H). HRMS(ESI): *m*/*z* calculated for $C_{22}H_{21}ClFN_5O_3 + H^+$ [M + H^+]: 458.1395. Found: 458.1370.

2-*tert*-Butyl 5-(4-(3-chloro-2-fluorophenylamino)-7-methoxyquinazolin-6-yl) 2,5-diazabicyclo[4.1.0]heptane-2,5-dicarboxylate (20). A mixture of *tert*-butyl 5-(chlorocarbonyl)-2,5-diazabicyclo[4.1.0]heptane-2-carboxylate (**19**) (5.2 g, crude, ~15.1 mmol), **6** (3.4 g, 10.6 mmol), and potassium carbonate (3.1 g, 22.7 mmol) in N,N-dimethylformamide (50 mL) was stirred at room temperature overnight. After the reaction was completed, the solvent was evaporated under reduced pressure. The residue was treated with water (100 mL). The solid was collected by filtration and dried *in vacuo* to afford **20** (5.85 g, crude). LCMS (ESI) *m*/*z* calculated for $C_{26}H_{27}ClFN_5O_5 + H^+$ [M+H^+]: 544.2. Found: 544.1.

4-(3-Chloro-2-fluorophenylamino)-7-methoxyquinazolin-6-yl 2,5-diazabicyclo[4.1.0]heptane-2-carboxylate (21). To a solution of **20** (5.85 g, crude) in ethyl acetate (20 mL) was added a solution of HCl in 1,4-dioxane (50 mL, 4.0 M). The reaction mixture was stirred at room temperature for 1 h, concentrated, and dried under vacumn to afford crude **21** (5.61 g) which was used for next step directly.

4-(3-Chloro-2-fluorophenylamino)-7-methoxyquinazolin-6-yl 5-methyl-2,5-diazabicyclo[4.1.0]heptane-2-carboxylate (22). To a solution of **21** (5.61 g, ~10 mmol) in methanol (50 mL) was added triethylamine (1.07 g, 10.6 mmol), paraformaldehyde (645 mg, 21.5 mmol) and acetic acid (1.29 g, 21.5 mmol). The resulting mixture was stirred at room temperature overnight. Then $NaBH_3CN$ (1.35 g, 21.5 mmol) was added and the reaction mixture was stirred at room temperature for additional 24 h. The solvent was evaporated and the residue was purified by reverse phase preparative HPLC using Gemini 250 x 50 mm column with 10 μm particle size and eluting with a gradient of 25-50% acetonitrile (containing 0.05% ammonia) in

water to provide **22** (2.0 g, 4.38 mmol, 41% for two steps) as a racemic mixture. LCMS (ESI) *m*/*z* calculated for $C_{22}H_{21}ClFN_5O_3 + H^+$ [M+H$^+$]: 458.1. Found: 458.0.

4-(3-Chloro-2-fluorophenylamino)-7-methoxyquinazolin-6-yl 5-methyl-2,5-diazabicyclo[4.1.0]heptane-2-carboxylate, isomer 1 (1i), and isomer 2 (1j). Racemic mixture **22** (0.99 g, 2.17 mmol) was separated by chiral supercritical fluid chromatography using AD 300 x 50 mm column and eluting with 40% methanol in ammonia to afford **1i** (isomer 1, 445 mg) and **1j** (isomer 2, 440 mg). Compounds **1i** and **1j** were separately treated with HCl aqueous solution (1.0 M, 1 mL) and lyophilized to provide HCl salt of **1i** (471.8 mg, 0.95 mmol, 44%) and HCl salt of **1j** (465.5 mg, 0.94 mmol, 43% yield), respectively. (Analytical method: Column: Chiralpak AD-3 50 x 4.6 mm with 3 μm particle size; mobile phase: methanol containing 0.05% di-ethylamine in CO_2 from 5% to 40%; flow rate: 4 mL/min; wavelength: 220 nm). HCl salt of **1i** (peak 1): t_R = 1.30 min in 4 min chromatography (t_R = 1.90 min in chiral SFC). ^{1}H NMR: (400MHz, CD_3OD) δ 8.59 (s, 1H), 8.28 (s, 1H), 7.60-7.57 (m, 1H), 7.51-7.47 (m, 1H), 7.36 (s, 1H), 7.30-7.26 (m, 1H), 4.18-4.00 (m, 1H), 4.08 (s, 3H), 3.53-3.46 (m, 1H), 3.37-3.10 (m, 3H), 3.01-2.93 (m, 1H), 2.95 (s, 3H), 1.41-1.14 (m, 2H). ^{13}C NMR (101 MHz, CD_3OD): δ 160.6, 159.2, 156.4, 154.7, 153.3, 147.8, 142.6, 142.4, 129.8, 127.9, 126.0, 122.9, 118.1, 109.6, 106.4, 57.4, 51.0, 43.9, 41.5, 38.5, 30.4, 9.7. HRMS (ESI): *m*/*z* calculated for $C_{22}H_{21}ClFN_5O_3 + H^+$ [M + H$^+$]: 458.1395. Found: 458.1401. HCl of **1j** (peak 2): t_R = 1.33 min in 4 min chromatography (t_R = 2.11 min in chiral SFC). ^{1}H NMR: (400 MHz, CD_3OD) δ 8.64 (s, 1H), 8.35 (s, 1H), 7.60-7.56 (m, 1H), 7.52-7.49 (m, 1H), 7.38 (s, 1H), 7.31-7.27 (m, 1H), 4.22-4.00 (m, 1H), 4.10 (s, 3H), 3.58-3.45 (m, 2H), 3.36-3.25 (m, 2H), 3.17-3.09 (m, 1H), 3.04 (s, 3H), 1.52-1.24 (m, 2H). ^{13}C NMR (101 MHz, CD_3OD): δ 160.9, 159.5, 155.8, 155.4, 154.3, 153.3, 146.6, 142.7, 130.1, 128.1,

126.0, 122.9, 118.4, 109.4, 105.7, 57.5, 51.1, 43.9, 41.1, 38.4, 30.6, 9.9. HRMS (ESI): *m*/*z* calculated for $C_{22}H_{21}ClFN_5O_3 + H^+$ [M + H^+]: 458.1395. Found: 458.1386.

(*S*)-4-(3-Chloro-2-fluorophenylamino)-7-methoxyquinazolin-6-yl 3,4-dimethylpiperazine-1-carboxylate (1k). A mixture of (*S*)-3,4-dimethylpiperazine-1-carbonyl chloride (**18f**) (5.8 g, ~10.15 mmol), **6** (2.6 g, 8.12 mmol) and potassium carbonate (4.2 g, 30.45 mmol) in DMF (120 mL) was stirred at room temperature for 16 h. After evaporation of solvent under vacuum, the residue was treated with water. The mixture was extracted with ethyl acetate (4 x 500 mL). The combined organic layers were dried over sodium sulfate and concentrated. The residue was purified by reverse phase preparative HPLC using Phenomenex Synergi 250 × 50 mm column with 10 μm particle size and eluting with a gradient of 5-25% acetonitrile (containing 0.2% formic acid) in water. The fractions contained desired product were neutralized with potassium carbonate, the precipitate was collected by filtration and dried *in vacuo* to provide **1k** (2460 mg). This compound was dissolved in CH_3CN (5 mL), treated with 1 N HCl (5.5 mL) and lyophilized to afford the HCl salt of **1k** (2647.1 mg, 5.34 mmol, 66%). ^{1}H NMR (400 MHz, CD_3OD): δ 8.79 (s, 1H), 8.50 (s, 1H), 7.60-7.53 (m, 2H), 7.43 (s, 1H), 7.34-7.30 (m, 1H), 4.53 (br, 1H), 4.32 (br, 1H), 4.14 (s, 3H), 3.84-3.22 (m, 5H), 3.04 (s, 3H), 1.52 (br, 3H). HRMS (ESI): *m*/*z* calculated for $C_{22}H_{23}ClFN_5O_3 + H^+$ [M + H^+]: 460.1552. Found: 460.1538.

(*R*)-4-(3-Chloro-2-fluorophenylamino)-7-methoxyquinazolin-6-yl 3,4-dimethylpiperazine-1-carboxylate (1l). A mixture of (*R*)-3,4-dimethylpiperazine-1-carbonyl chloride (**18g**) (6.2 g, ~13.4 mmol), **6** (3.56 g, 11.12 mmol) and potassium carbonate (5.76 g, 41.7 mmol) in DMF (100 mL) was stirred at room temperature for 16 h. The mixture was concentrated *in vacuo* and treated with water. The mixture was then extracted with ethyl acetate (4 x 500 mL). The combined organic layers were dried over sodium sulfate and concentrated. The residue was

purified by reverse phase preparative HPLC using Synergi Phenomenex Synergi 250 × 50 mm column with 10 μm particle size and eluting with a gradient of 2-40% acetonitrile (containing 0.2% formic acid) in water. The fractions contained desired product were neutralized with potassium carbonate, the precipitate was collected by filtration and dried *in vacuo* to provide **1l** (2500 mg). Compound **1l** was dissolved in CH_3CN (5 mL), treated with 1 N HCl (5.5 mL) and lyophilized to afford the HCl salt of **1l** (2663.6 mg, 5.37 mmol, 48%). ^{1}H NMR (400 MHz, D_2O): δ 8.38 (s, 1H), 7.84 (s, 1H), 7.51-7.44 (m, 2H), 7.27-7.23 (m, 1H), 7.06 (s, 1H), 4.34 (br, 1H), 4.23 (br, 1H), 3.92 (s, 3H), 3.68-3.48 (m, 2H), 3.45-3.15 (m, 3H), 2.99 (s, 3H), 1.41 (d, J = 4.8 Hz, 3H). HRMS (ESI): m/z calculated for $C_{22}H_{23}ClFN_5O_3$ + H^+ [M + H^+]: 460.1552. Found: 460.1539.

(*R*)-4-*tert*-Butyl 1-(4-(2-fluorophenylamino)-7-methoxyquinazolin-6-yl) 2-methylpiperazine-1,4-dicarboxylate (23). A mixture of **8** (15.8 g, ~60 mmol), **6** (19.2 g, 60 mmol), and potassium carbonate (16.6 g, 120 mmol) in dry N, N-dimethylformamide (300 mL) was stirred overnight at room temperature. The reaction mixture was poured into water (250 mL) and filtered. The filtration cake was dried under vacuum to afford crude **23** (25 g) as yellow solid, which was used without further purification. HRMS (ESI) m/z calculated for $C_{26}H_{29}ClFN_5O_5$+ H^+ [M+H^+]: 546.1914. Found: 546.1901.

(*R*)-4-(3-Chloro-2-fluorophenylamino)-7-methoxyquinazolin-6-yl 2-methylpiperazine-1-carboxylate (24). HCl in dioxane (4M, 1 L) was added to a solution of **23** (750 g, crude) in methanol (1.0 L). The mixture was stirred at room temperature for 1 h and concentrated. The residue was diluted with water (3 L) and neutralized to pH = 7 with saturated sodium bicarbonate solution. After filtration, the collected solid was treated with toluene (300 mL) and the toluene was evaporated under reduced pressure. This process was repeated twice and the crude

compound **24** (495 g, yellow solid) was used without further purification. HRMS (ESI) calculated for $C_{21}H_{21}ClFN_5O_3+H^+$ [M+H$^+$]: 446.1390. Found: 446.1393.

4-[(3-Chloro-2-fluorophenyl)amino]-7-methoxyquinazolin-6-yl (2*R*)-2,4-dimethylpiperazine-1-carboxylate (1m). Sodium cyanoborohydride (2.0 g, 32 mmol) was added to a mixture of **24** (8 g, ~15 mmol) and paraformaldehyde (1.0 g, 32 mmol) in methanol (100 mL). The reaction mixture was stirred at room temperature overnight and then concentrated *in vacuo*. The residue was treated with water and extracted with ethyl acetate (3 x 100 mL). The combined organic layers were washed with brine, dried over anhydrous sodium sulfate, and concentrated under reduced pressure. The crude product was purified by reverse phase preparative HPLC using Synergi 250 x 77 mm column with 10 μm particle size and eluting with a gradient of 5-35% acetonitrile (containing 0.05% formic acid) in water. The combined desired fractions were neutralized with saturated potassium carbonate and concentrated under reduced pressure. The residue was extracted with ethyl acetate (3 x 100 mL). The combined organic layers were concentrated *in vacuo* and freeze-dried to afford **1m** (4.0 g, 8.71 mmol, 58%) as white solid. ^{1}H NMR (400 MHz, $CDCl_3$): δ 8.76 (s, 1H), 8.53-8.48 (m, 1H), 7.65 (s, 1H), 7.44 (br, 1H), 7.34 (s, 1H), 7.19 - 7.15 (m, 2H), 4.51-4.50 (br, 1H), 4.20-4.05 (br, 1H), 3.99 (s, 3H), 3.50-3.30 (br, 1H), 2.87 (d, J = 10.8 Hz, 1H), 2.73 (d, J = 11.2 Hz, 1H), 2.35 (s, 3H), 2.35-2.25 (m, 1H), 2.13-2.11 (m, 1H), 1.47 (br, 3H). ^{13}C NMR (101 MHz, DMSO-d_6): δ 158.1, 156.7, 155.2, 154.2, 153.0, 151.7, 150.4, 140.4, 128.6, 127.8, 127.4, 125.4, 120.7, 116.9, 108.8, 59.5, 56.8, 55.0, 48.3, 46.4, 16.6. HRMS (ESI) calculated for $C_{22}H_{23}ClFN_5O_3$+ H$^+$ [M+H$^+$]$^+$ 460.1546. Found: 460.1540.

4-[(3-Chloro-2-fluorophenyl)amino]-7-methoxyquinazolin-6-yl (2*S*)-2,4-dimethylpiperazine-1-carboxylate (1n). A mixture of **6** (150 mg, 0.47 mmol), (*S*)-2,4-

dimethylpiperazine-1-carbonyl chloride (**18h**) (1 g, crude) and K_2CO_3 (130 mg, 0.94 mmol) in DMF (10 mL) was stirred at 30 °C overnight. The mixture was cooled to room temperature, treated with water, and filtered. The filtration cake was purified by reverse phase preparative HPLC using ASB 150 x 25 mm column with 5 μm particle size and eluting with a gradient of 3-28% acetonitrile (containing 0.05% HCl) in water to give HCl salt of **1n** (21.0 mg, 0.042 mmol, 9%). ^{1}H NMR (400 MHz, CD_3OD): δ 8.77 (s, 1H), 8.43 (s, 1H), 7.57-7.50 (m, 2H), 7.38 (s, 1H), 7.32-7.28 (m, 1H), 4.51-4.21 (m, 1H), 4.10 (s, 3H), 3.77-3.35 (m, 5H), 3.27-3.17 (m, 1H), 2.99 (s, 3H), 1.58-1.49 (m, 3H). LCMS (ESI): *m/z* calculated for $C_{22}H_{23}ClFN_5O_3$ + H^+ [M + H^+]: 460.1. Found: 460.1.

▪ ASSOCIATED CONTENT

Supporting Information. EGFR inhibition activity of compounds **1a-n** and **2** in biochemical assay; cellular assay data of compounds **1a-n** and **2**; biochemical assay protocols; cellular phosphorylation and proliferation assay procedures; permeability and efflux transport in MDCKII-MDR1 and MDCK-BCRP cell lines; unbound brain to unbound blood ($K_{puu,brain}$) and CSF to unbound blood ($K_{puu,CSF}$) ratios; compound **1e** hepatocyte metabolite ID; Millipore kinase panel screening results; secondary pharmacology panel screening results; PET microdosing study; summary of *in vitro* DMPK of **1m**; metabolites identified in rat, dog, monkey, and human hepatocytes; physical properties of **1m**; procedures for assessing pEGFR expression in tumor tissue by using immunohistochemistry; tumor growth curve of individual animals. This material is available free of charge via the Internet at http://pubs.acs.org.

▪ AUTHOR INFORMATION

Corresponding Author

* Phone: +86 21 61097888. Fax: +86 21 61097711. Email: xiaolin.zhang@astrazeneca.com

▪ ACKNOWLEDGMENT

We thank the chemistry team at WuXi AppTec for collaboration, biology and DMPK groups at Innovation Center China (ICC), AstraZeneca, for generating data to support the project, Drs. Les Hughes, David Wilson, Honchung Tsui, Anne Galer at AstraZeneca for proof reading of this manuscript, Ms. Nanyan Zhou for data management.

▪ ABBREVIATIONS

EGFR, epidermal growth factor receptor; EGFR TKI, epidermal growth factor receptor tyrosine kinase inhibitor; NSCLC, non-small cell lung cancer; BBB, blood-brain-barrier; BM, brain metastasis; LM, leptomeningeal metastasis; CNS, central nervous system; MDCK, Madin-Darby canine kidney; MDR1, multidrug resistance protein 1; BCRP, breast cancer resistance protein; Pgp, P-glycoprotein; PSA, polar surface area; CSF, cerebrospinal fluid; PK, pharmacokinetics; wt, wild-type; ATP, adenosine triphosphate; OATP, organic anion-transporting polypeptide; DDI, drug-drug interaction; EGFR TK, EGFR tyrosine kinase; Cl_{int}, intrinsic clearance; $CL_{hepatic}$, hepatic clearance; IVIVe: *in vitro-in vivo* extrapolation; LBF: liver blood flow method; PET, positron emission tomography; LCMS, liquid chromatography-mass spectrometry; SAR, structure-activity relationship; HPLC, high-performance liquid chromatography; SFC, supercritical fluid chromatography; MS, mass spectrometry; DCM, dichloromethane; DMF, N,N-dimethylformamide; DMSO, dimethyl sulfoxide; TFA, trifluoroacetic acid; THF, tetrahydrofuran; rt, room temperature; h, hour(s); t_R, retention time.

▪ REFERENCES

(1) Molina, J. R.; Yang, P.; Cassivi, S. D.; Schild, S. E.; Alex, A.; Adjei, A. A. Non–small cell lung cancer: epidemiology, risk factors, treatment, and survivorship. *Mayo Clin. Proc*. **2008**, *83*, 584–594.

(2) Siegel, R.; Ma, J.; Zou, Z; Jemal, A. Cancer Statistics, 2014. *CA Cancer J. Clin*. **2014**, *64*, 9–22.

(3) Sharma, S. V.; Bell, D. W.; Settleman, J.; Haber, D. A. Epidermal growth factor receptor mutations in lung cancer. *Nat. Rev. Cancer*. **2007**, *7*, 169−181.

(4) Mok, T. S.; Wu, Y.-L.; Thongprasert, S.; Yang, C.-H.; Chu, D.-T.; Saijo, N.; Sunpaweravong, P.; Han, B.; Margono, B.; Ichinose, Y.; Nishiwaki, Y.; Ohe, Y.; Yang, J.-J.; Chewaskulyong, B.; Jiang, H.; Duffield, E. L.; Watkins, C. L.; Armour, A. A.; Fukuoka, M. Gefitinib or carboplatin-paclitaxel in pulmonary adenocarcinoma. *N. Engl. J. Med*. **2009**, *361*, 947-957.

(5) Shepherd, F. A.; Pereira, J. R.; Ciuleanu, T.; Tan, E. H.; Hirsh, V.; Thongprasert, S.; Campos, D.; Maoleekoonpiroj, S.; Smylie, M.; Martins, R.; Kooten, M. V.; Dediu, M.; Findlay, B.; Tu, D.; Johnston, D.; Bezjak, A.; Clark, G.; Santabarbara, P.; Seymour, L. Erlotinib in previously treated non-small-cell lung cancer. *N. Engl. J. Med*. **2005**, *353*, 123-132.

(6) Cataldo, V. D.; Gibbons, D. L.; Pérez-Soler, R.; Quintás-Cardama, A. Treatment of non–small-cell lung cancer with erlotinib or gefitinib. *N. Engl. J. Med*. **2011**, *364*, 947-955.

(7) Wu, Y.-L.; Zhou, C.; Hu, C.-P.; Feng, J.; Lu, S.; Huang, Y.; Li, W.; Hou, M.; Shi, J. H.; Lee, K.-Y.; Xu, C. R.; Massey, D.; Kim, M.; Shi, Y.; Geater, S. L. Afatinib versus cisplatin plus gemcitabine for first-line treatment of Asian patients with advanced non-

small-cell lung cancer harbouring EGFR mutations (LUX-Lung 6): an open-label, randomised phase 3 trial. *Lancet Oncol*. **2014**, *15*, 213-222.

(8) Barajas, R. F. Jr.; Cha, S. Imaging diagnosis of brain metastasis. *Prog. Neurol. Surg*. **2012**, *25*, 55–73.

(9) Nguyen, N. P.; Nguyen, M. L.; Vock, J.; Lemanski, C.; Kerr, C.; Vinh-Hung, V.; Chi, A.; Khan, R.; Woods, W.; Altdorfer, G.; D'Andrea, M.; Karlsson, U.; Hamilton, R.; Ampil, F. Potential applications of imaging and image-guided radiotherapy for brain metastases and glioblastoma to improve patient quality of life. *Front. Oncol*. **2013**, *3*, Article 284.

(10) Nayak, L.; Lee, E. Q.; Wen, P. Y. Epidemiology of brain metastases. *Curr. Oncol. Rep*. **2012**, *14*, 48–54.

(11) Gril, B.; Evans, L.; Palmieri, D.; Steeg, P. S. Translational research in brain metastasis is identifying molecular pathways that may lead to the development of new therapeutic strategies. *Eur. J. Cancer*, **2010**, *46*, 1204–1210.

(12) Grommes, C.; Oxnard, G. R.; Kris, M. G.; Miller, V. A.; Pao, W.; Holodny, A. I.; Clarke, J. L.; Lassman, A. B. "Pulsatile" high-dose weekly erlotinib for CNS metastases from EGFR mutant non-small cell lung cancer. *Neuro-Oncology*, **2011**, *13*, 1364–1369.

(13) Jackman, D. M.; Holmes, A. J.; Lindeman, N.; Wen, P. Y.; Kesari, S.; Borras, A. M.; Bailey, C.; Jong, F. D.; Jänne, P. A.; Johnson, B. E. Response and resistance in a non–small-cell lung cancer patient with an epidermal growth factor receptor mutation and leptomeningeal metastases treated with high-dose gefitinib. *J. Clin. Oncol*. **2006**, *24*, 4517-4520.

(14) Owonikoko, T. K.; Arbiser, J.; Zelnak, A,; Shu, H.-K. G.; Shim, H.; Robin, A. M.; Kalkanis, S. N.; Whitsett, T. G.; Salhia, B.; Tran, N. L.; Ryken, T.; Moore, M. K.; Egan, K. M.; Jeffrey, J.; Olson, J. J. Current approaches to the treatment of metastatic brain tumours. *Nat. Rev. Clin. Oncol.* **2014**, *11*, 203–222.

(15) Gow, C.-H.; Chien, C.-R.; Chang, Y.-L.; Chiu, Y.-H.; Kuo, S.-H.; Shih, J.-Y.; Chang, Y.-C.; Yu, C.-J.; Yang, C.-H.; Yang, P.-C. Radiotherapy in lung adenocarcinoma with brain metastases: effects of activating epidermal growth factor receptor mutations on clinical response. *Clin. Cancer Res*. **2008**, *14*, 162-168.

(16) Pardridge, W. M. The blood-brain barrier: bottleneck in brain drug development. *NeuroRx*, **2005**, *2*, 3-14.

(17) Löscher, W.; Potschka, H. Blood-brain barrier active efflux transporters: ATP-binding cassette gene family. *NeuroRx*. **2005**, *2*, 86–98.

(18) Mahringer, A.; Ott, M.; Reimold, I.; Reichel, V.; Fricker, G. The ABC of the blood-brain barrier-regulation of drug efflux pumps. *Current Pharmaceutical Design*, **2011**, *17*, 2762-2770.

(19) Mahar Doan, K. M.; Humphreys, J. E.; Webster, L. O.; Wring, S. A.; Shampine, L. J.; Serabjit-Singh, C. J.; Adkison, K. K.; Polli, J. W. Passive permeability and P-glycoprotein-mediated efflux differentiate central nervous system (CNS) and non-CNS marketed drugs. *J. Pharmacol. Exp. Ther*. **2002**, *303*, 1029–1037.

(20) Wager, T. T.; Villalobos, A.; Verhoest, P. R.; Hou, X.; Shaffer, C. L. Strategies to optimize the brain availability of central nervous system drug candidates. *Expert Opin. Drug Discov*. **2011**, *6*, 371-381.

(21) Hitchcock, S. A.; Pennington, L. D. Structure-brain exposure relationships. *J. Med. Chem*. **2006**, *49*, 7559-7583.

(22) Ghose, A. K.; Herbertz, T.; Hudkins, R. L.; Dorsey, B. D.; Mallamo, J. P. Knowledge-based, central nervous system (CNS) lead selection and lead optimization for CNS drug discovery. *ACS Chem. Neurosci*. **2012**, *3*, 50−68.

(23) Rankovic, Z. CNS drug design: balancing physicochemical properties for optimal brain exposure. *J. Med. Chem.*, **2015**, *58*, 2584–2608.

(24) Yun, C.-H.; Boggon, T. J.; Li, Y.; Woo, M. S.; Greulich, H.; Meyerson, M.; Eck, M. J. Structures of lung cancer-derived EGFR mutants and inhibitor complexes: mechanism of activation and insights into differential inhibitor sensitivity. *Cancer Cell*. **2007**, *11*, 217-227.

(25) Ballard, P.; Bradbury, R. H.; Harris, C. S.; Hennequin, L. F. A.; Hickinson, M.; Kettle, J. G.; Kendrew, J.; Klinowska, T.; Ogilvie, D. J.; Pearson, S. E.; Williams, E. J.; Wilson, I. Inhibitors of epidermal growth factor receptor tyrosine kinase: optimisation of potency and in vivo pharmacokinetics. *Bioorg. Med. Chem. Lett*. **2006**, *16*, 4908–4912.

(26) Pankratov, A, N.; Shalabay, A. V. Effect of the intramolecular hydrogen bond on the electronic structure of the organic molecules with a planar quasicycle. *J. Structural Chem*. **2007**, *48*, 427-432.

(27) Galan, J. F.; Brown, J.; Wildin, J. L; Liu, Z.; Liu, D.; Moyna, G.; Pophristic, V. Intramolecular hydrogen bonding in *ortho*-substituted arylamide oligomers: a computational and experimental study of *ortho*-fluoro- and ortho-chloro-N-methylbenzamide. *J. Phys. Chem. B* **2009**, *113*, 12809-12815.

(28) Weiss, M. M.; Williamson, T.; Babu-Khan, S.; Bartberger, M. D.; Brown, J.; Chen, K.; Cheng, Y.; Citron, M.; Croghan, M. D.; Dineen, T. A.; Esmay, J.; Graceffa, R. F.; Harried, S. S.; Hickman, D.; Hitchcock, S. A.; Horne, D. B.; Huang, H.; Imbeah-Ampiah, R.; Judd, T.; Kaller, M. R.; Kreiman, C. R.; La, D. S.; Li, V.; Lopez, P.; Louie, S.; Monenschein, H.; Nguyen, T. T.; Pennington, L. D.; Rattan, C.; San Miguel, T.; Sickmier, E. A.; Wahl, R. C.; Wen, P. H.; Wood, S.; Xue, Q.; Yang, B. H.; Patel, V. F.; Zhong, W. Design and preparation of a potent series of hydroxyethylamine containing β-secretase inhibitors that demonstrate robust reduction of central β-amyloid. *J. Med. Chem*. **2012**, *55*, 9009-9024.

(29) Liu, X.; Smith, B. J.; Chen, C.; Callegari, E.; Becker, S. I.; Chen, X.; Cianfrogna, J.; Doran, A. C.; Doran, S. D.; Gibbs, J. P.; Hosea, N.; Liu, J.; Nelson, F. R.; Szewc, M. A.; Deusen, J. V. Evaluation of cerebrospinal fluid concentration and plasma free concentration as a surrogate measurement for brain free concentration. *Drug Metab. Dispos*. **2006**, *34*, 1443-1447.

(30) Di, L.; Rong, H.; Feng, B. Demystifying brain penetration in central nervous system drug discovery. *J. Med. Chem*. **2013**, *56*, 2–12.

(31) Riley, R. J.; McGinnity, D. F.; Austin, R. P. A unified model for predicting human hepatic, metabolic clearance from in vitro intrinsic clearance data in hepatocytes and microsomes. *Drug Metab. Dispos*. **2005**, *33*, 1304-1311.

(32) Sohlenius-Sternbeck, A. K.; Jones, C.; Ferguson, D.; Middleton, B. J.; Projean, D.; Floby, E.; Bylund, J.; Afzelius, L. Practical use of the regression offset approach for the prediction of in vivo intrinsic clearance from hepatocytes. *Xenobiotica*, **2012**, *42*, 841-853.

(33) Mahmood, I. Prediction of clearance in humans from in vitro human liver microsomes and allometric scaling. A comparative study of the two approaches. *Drug Metab. Drug Interact*. **2002**, *19*, 49–64.

(34) Mahmood, I. Prediction of human drug clearance from animal data: Application of the rule of exponent and fu corrected intercept method (FCIM). *J. Pharm. Sci*. **2006**, 95, 1810–1821.

(35) Ward, K. W.; Smith, B. R. A comprehensive quantitative and qualitative evaluation of extrapolation of intravenous pharmacokinetic parameters from rat, dog and monkey to humans. I. Clearance. *Drug Metab. Dispos*. **2004**, *32*, 603–611.

(36) FDA guidance for industry (2012) on drug interaction studies-study design, data analysis, implications for dosing, and labeling recommendations: http://www.fda.gov/downloads/Drugs/GuidanceComplianceRegulatoryInformation/Guidances/ucm292362.pdf

(37) Fahmi, O. A.; Kish, M.; Boldt, S.; Obach, R. S. Cytochrome P450 3A4 mRNA is a more reliable marker than CYP3A4 activity for detecting pregnane X receptor-activated induction of drug metabolizing enzymes. *Drug Metab. Dispos*. **2010**, *38*, 1605-1611.

(38) Katarina Varnäs, K; Varrone, A.; Farde, L. Modeling of PET data in CNS drug discovery and development. *J. Pharmacokinet. Pharmacodyn*. **2013**, *40*, 267–279.

(39) Di, L.; Umland, J. P.; Chang, G.; Huang, Y.; Lin Z.; Scott, D. O.; Troutman, M. D.; Liston, T. E. Species independence in brain tissue binding using brain homogenates. *Drug. Metab. Dispos.* **2011**, *39*, 1270-1277.

(40) Helal, C. J.; Kang, Z.; Hou, X.; Pandit, J.; Chappie, T. A.; Humphrey, J. M.; Marr, E. S.; Fennell, K. F.; Chenard, L. K.; Fox, C.; Schmidt, C. J.; Williams, R. D.; Chapin, D.

S.; Siuciak, J.; Lebel, L.; Menniti, F.; Cianfrogna, J.; Fonseca, K. R.; Nelson, F. R.; O'Connor, R.; MacDougall, M.; McDowell, L.; Liras, S. Use of structure-based design to discover a potent, selective, in vivo active phosphodiesterase 10a inhibitor lead series for the treatment of schizophrenia. *J. Med. Chem*. **2011**, *54*, 4536–4547.

(41) Chen, Y.; Feng, M.; Li, S.; Xu, J.; Ning, H.; He, Y.; Wang, X.; Ding, R.; Qi, C. Synthesis and evaluation of novel F-18 labeled 4-aminoquinazoline derivatives: Potential PET imaging agents for tumor detection. *Bioorg. Med. Chem. Lett*. **2012**, *22*, 4745–4749.

(42) Rice, K. D.; Gangloff, A. R.; Kuo, E. Y.-L.; Dener, J. M.; Wang, V. R.; Lum, R.; Newcomb, W. S.; Havel, C.; Putnam, D.; Cregar, L.; Wong, M.; Warne, R. L. Dibasic inhibitors of human mast cell tryptase. part 1: synthesis and optimization of a novel class of inhibitors. *Bioorg. Med. Chem. Lett*. **2000**, *10*, 2357-2360.

(43) Chen, L.; Tilley, J.; Trilles, R. V.; Yun, W.; Fry, D.; Cook, C.; Rowan, K,; Schwinge, V.; Campbell, R. N-Acyl-L-phenylalanine derivatives as potent VLA-4 antagonists that mimic a cyclic peptide conformation. *Bioorg. Med. Chem. Lett*. **2002**, *12*, 137–140.

(44) Kemper, E. M.; Leenders, W.; Küsters, B.; Lyons, S.; Buckle, T.; Heerschap, A.; Boogerd, W.; Beijnen, J. H.; van Tellingen, O. Development of luciferase tagged brain tumour models in mice for chemotherapy intervention studies. *Eur. J. Cancer*. **2006**, *42*, 3294-3303.

(45) Lal, S.; Lacroix, M.; Tofilon, P.; Fuller, G. N.; Sawaya, R.; Lang, F, F. An implantable guide-screw system for brain tumor studies in small animals. *J. Neurosurg.* **2000**, *92*, 326-333.